Time-domain analyses of the layered soil by the modified scaled boundary finite element method

Shan Lu[1a], Jun Liu[*1,2,3], Gao Lin[1b] and Wenyuan Wang[1c]

[1]*School of Hydraulic Engineering, Faculty of Infrastructure Engineering, Dalian University of Technology, China*
[2]*State Key Laboratory of Structural Analysis for Industrial Equipment, Dalian University of Technology, Dalian 116024, China*
[3]*State Key Laboratory of Coastal and Offshore Engineering, Dalian University of Technology, Dalian 116024, China*

Abstract.   The dynamic response of two-dimensional unbounded domain on the rigid bedrock in the time domain is numerically obtained. It is realized by the modified scaled boundary finite element method (SBFEM) in which the original scaling center is replaced by a scaling line. The formulation bases on expanding dynamic stiffness by using the continued fraction approach. The solution converges rapidly over the whole time range along with the order of the continued fraction increases. In addition, the method is suitable for large scale systems. The numerical method is employed which is a combination of the time domain SBFEM for far field and the finite element method used for near field. By using the continued fraction solution and introducing auxiliary variables, the equation of motion of unbounded domain is built. Applying the spectral shifting technique, the virtual modes of motion equation are eliminated. Standard procedure in structural dynamic is directly applicable for time domain problem. Since the coefficient matrixes of equation are banded and symmetric, the equation can be solved efficiently by using the direct time domain integration method. Numerical examples demonstrate the increased robustness, accuracy and superiority of the proposed method. The suitability of proposed method for time domain simulations of complex systems is also demonstrated.

Keywords: scaled boundary finite element method; multilayered unbounded domain; continued fraction approach; time domain analysis

1. Introduction

Structure foundation dynamic interaction has been an active research topic for years. This problem has been required in many fields of engineering, such as dam-reservoir systems, high buildings, transportation and pile foundation. The effect of structure foundation dynamic

∗Corresponding author, Lecturer, E-mail: liujun8128@126.com, liujun8128@dlut.edu.cn
[a]Ph.D., E-mail: coolgirl86@163.com
[b]Professor, E-mail: gaolin@dlut.edu.cn
[c]Ph.D. Student, E-mail: wangwenyuan@dlut.edu.cn

interaction is recognized as important and can not be neglected. For the view of engineering application, it is necessary to study the structure foundation dynamic interaction topic. Its origins can be traced back to the late 19th century (Sung 1953, Bycroft 1956, Richart and Whitman 1967). In most cases, the soil is multilayered due to sedimentation process. Therefore the multilayered soil is a complex analysis model (Murakami *et al*. 1996). Therefore, studying the dynamic response problem of multilayered soil, it is a more significant topic. Several numerical approaches have been present to solve this subject. The finite element method (FEM) is the original and effective method for the numerical analysis to solve the subject. The problem domain is divided into many small elements. The dynamic property is modeled by the static stiffness matrix, mass matrix and damping matrix. The unbounded domain is modeled by using viscous-spring artificial boundaries method (Liu *et al*. 2006, Deeks and Randolph 1994). Some commercial finite element software can solve the large engineering problems. However, the solving process consumes a large amount of computation times and human efforts. Many techniques which are required for the time domain analysis have been applied to reduce the computation times and human efforts recently. Such as high-order elements are successfully applied in fluid dynamics, and Gauss-Lobatto-Legendre polynomials are introduced to shape functions (Komatitsch and Tromp 2002) which lead to the equations with sparse coefficient matrix and can be easily storage. The boundary element method (BEM) (Beskos 1987, Hall and Oliveto 2003) satisfies the motion equation of problem domain and the boundary condition at infinity automatically by using fundamental solution. This method has advantage in meshing generation and simplifying the model construction. Only the boundary is discretized yielding a reduction of the spatial dimension by one. However, in order to obtain the fundamental solution in time domain, the convolution integrals have to be evaluated and the solving process consumes a large amount of computation times. Specially, it is very complicated to solve the fundamental solution for the anisotropic problem domain problem. The thin layer method (Kausel and Roesset 1975, Kausel and Peek 1982, Kausel 1986, Seale 1989, Kausel 1994) is suitable for solving the dynamic analysis of the horizontally layered media. This method can construct exact non-reflecting boundary condition by the analytical solutions of the unbounded domain. The limit of this method is that the analytical solutions are only suitable for simple geometries. Recently, the analytical layer element method (Ai and Feng 2014, Ai and Cang 2012, Ai and Li 2014, Ai and Zhang 2015, Ai and Cheng 2011) has been developed. This method can be applied to solve the global stiffness matrix which is a diagonally dominant symmetric matrix and only associated with negative exponentials and the material properties. The characteristics of the global stiffness matrix lead to the solution process avoid overflow. It greatly improves the computational efficiency and the precision, especially for the multilayered soils. It also simplifies the whole calculation process.

The scaled boundary finite element method (SBFEM) (Wolf 2003) is a novel method which is expressly suitable for dynamic/static analysis of the unbounded domain for arbitrary geometry. The SBFEM is a semi analytical method which is adept at modeling wave propagation problems in unbounded domain and singular problems in bounded domain. The SBFEM overcomes the drawbacks of the FEM and BEM. This method automatically satisfies the radiation condition at infinity, while no fundamental solution (Song and Wolf 2000) and no artificial boundary conditions are needed. In the SBFEM, only the boundary is discretized. Thus, the dimension of problem domain is reduced by one. The anisotropy layered medium also can be modeling by the SBFEM without any difficulty. All of the above features of the SBFEM illustrate that the SBFEM has emerged as a promising numerical method.

Song and Wolf (Song and Wolf 1995, 1996, 1997, 2000, 2004) are the pioneers to derive the

SBFEM, and then they successfully solve the structure dynamic analysis in the frequency domain by the proposed method. In the subsequent researches, most analyses were forced on solving the dynamic stiffness in frequency domain (Birk and Prempramorte 2012, Birk and Behnke 2012.). This method also has been applied successfully in time domain. The original time domain analysis method was based on integrating the unit impulse response matrix, and thus it is computationally expensive. In view of this, many researchers have sought to solve the computational efficiency problem. Zhang (1999) introduced a linear approximated method for solving unit impulse response matrix. This method makes the computer time be reduced to considerably. Later, Yan and Zhang (2004) modified the solving process of the convolution integral by employing linear system theory. The unit impulse response matrix is expanded as a series of time independent matrices. Radmanovic and Katz (2010) proposed a high performance SBFEM based on an efficient integral method. Genes (2012), Schauer (2012) studied on the parallel computation for the large scale problems. In a word, most of the researchers are involved in improving the computational efficiency of dynamic analysis for the time domain problem. However, the dynamic analysis of layered medium is comparatively complex. For the view point of the engineering application, it is necessary to research on the dynamic response of layered medium in the time domain. But above reaches are all based on solving the unit impulse response matrix, and this solving method consumes a lot of computing time to solve the convolution integral. To increase the computational efficiency for the problems in the time domain, novel solution method has been proposed recently. Song and Bazyar (2007) developed a Padé series solution for the dynamic analysis of the unbounded domain. Song (2011) introduced the continued fraction method for the dynamic stiffness of the bounded domain starting from the SBFEM. It leads to the unbounded domain equation can be coupled seamlessly with the finite element equation. Birk *et al*. (2010) developed an high-order doubly asymptotic boundary by using doubly continued fraction method in acoustic and diffusion problems, respectively. Lin and Liu (2011) employed the continued fraction method to solve the waveguide eigenvalue problem successfully. Birk and Song (2009) presented a heat diffusion analysis in time domain by using the continued fraction method. Then, Chen and Birk (2014) proposed the continued fraction solution in bounded/unbounded domain. This method includes not only the static stiffness matrix and mass matrix but also the internal variables expressing the dynamic property at high frequencies. The continued fraction solution is applied in the equation of motion. It is expressed by the symmetric, sparse and high order static stiffness and mass matrices. Standard procedure in structural dynamic is directly applicable for solving time domain problem. The solving process of unit-impulse response matrix does not to be required, and it not only considerable improved the computational efficiency but also suitable for calculating the large scale models. Therefore, it is very suitable for making use of continued fraction to solve dynamic response. The objective of this paper is to develop a continued fraction solution directly from the SBFE equation for the semi unbounded layered medium with bedrock. Deriving the continued fraction solution of dynamic stiffness for the frequency domain, the equation of motion is a standard two order ordinary differential equation. We transform it into a first order ordinary differential equation. Applying the spectral shifting technique (Trinks 2004), the instability of the first order equation is removed before solving the equation. This paper introduces a direct time domain integration method (Adhikari and Wagner 2004) to solve the first order equation. Theinteger method makes computation linearly increase with order. It greatly improves the efficiency of calculation.

   This paper is organized as follows. In section 2, the modified SBFEM is summarized. It contains transforming coordinate, establishing displacement equation and establishment of the

(a) 2D layered medium

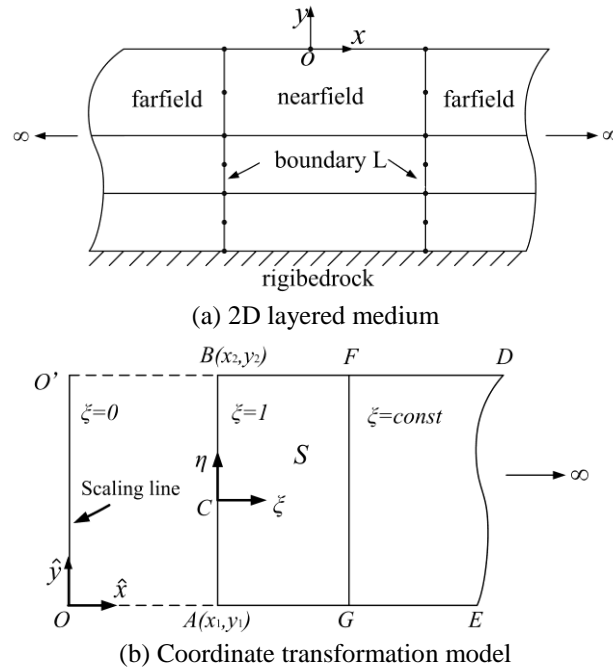(b) Coordinate transformation model

Fig. 1 Scaled boundary finite element method for 2D layered medium

dynamic stiffness equation. In section 3, the continued fraction solution of dynamic stiffness is introduced. In section 4, the SBFE equation of motion of the unbounded domain in time domain is constructed by introducing auxiliary variables. In section 5, the equation of motion is coupled with FEM seamlessly. In section 6, numerical examples are performed to demonstrate the accuracy and high efficiency of the present method, and the other examples are given to discuss the influences of the multilayer, the soft soil layer and the material parameters. In sections 6.1 and 6.2, we introduce the single and multi-layered medium by the rigid bedrock, respectively. They demonstrate the accuracy of the present method. In sections 6.3 and 6.4, we discussed the influence of the soft soil layer and the material parameters. Finally, the influence of loading form was analysed. At last, conclusion remarks are stated in section 7.

2. Summary of the 2D modified scaled boundary finite element method

The derivation of the modified scaled boundary finite element equation for the frequency domain is detailed introduced in Reference (Birk *et al.* 2012). Only the main process is introduced in this section. The new developments in this paper will be detailed in section 2.2.

2.1 Scaled boundary transformation of geometry coordinate

Consider a 2D medium with bedrock as shown in Fig. 1(a). Presuming each layer extends to infinity in horizontal direction, the soil layers are divided into near field which contains the upper structure and foundation and remaining the semi unbounded field is far field. It is similar to the

substructure method in soil-structure interaction analysis. Near field is modeled by the finite element method. Far field is analyzed by using the modified SBFEM which is derived in section 2.2. The boundary of near field /far field is vertical to the horizontal layer and rigid base, and the boundary is denoted as boundary L. The Cartesian coordinate is introduced such as that $\hat{x}$ axis is horizontal and the $\hat{y}$ axis is vertical, respectively. ($\hat{x}$, $\hat{y}$) and (x, y) are expressed as the point in the space and the point on the boundary L, respectively. The nodes on the boundary are reserved for the discrete boundary. The scaling centre in the original SBFEM is replaced by a vertical line-the scaling line, which coincides with $\hat{y}$ axis. As shown in Fig. 1(b), two scaled boundary coordinates ξ and η are introduced to describe the layered 2D unbound domain. The dimensionless coordinate ξ can be interpreted as a series of lines which are the parallel with the OO' axis. The unbounded domain S is composed by rays which pass through the scaling line and parallel to the $\hat{x}$ axis. The radial coordinate $\xi=1$ on the boundary L. The unbounded domain S is thus specified by $\xi>1$. The unbounded domain is obtained by the scaling radial coordinate of the boundary L, whereas the vertical coordinates are retained.

The coordinates $\hat{x}$, $\hat{y}$ are obtained by using shape function $N(\eta)$ to interpolate node coordinates x, y. According to the similarity between the boundary and line FG, the scaled boundary coordinate transformation is formulated as Eq. (1).

$$\begin{cases} \hat{x}(\xi,\eta) = N(\eta)\hat{x}(\xi) = \xi N(\eta)x \\ \hat{y}(\xi,\eta) = N(\eta)\hat{y}(\xi) = N(\eta)y \end{cases} \tag{1}$$

The partial derivatives with respect to the scaled boundary coordinates are expressed as

$$\begin{Bmatrix} \partial/\partial\xi \\ \partial/\partial\eta \end{Bmatrix} = \hat{J}(\xi,\eta) \begin{Bmatrix} \partial/\partial\hat{x} \\ \partial/\partial\hat{y} \end{Bmatrix} \tag{2}$$

where $\hat{J}(\varepsilon,\eta)$ is the Jacobian matrix, it is defined as

$$\hat{J}(\xi,\eta) = \begin{bmatrix} \hat{x}_{,\xi} & \hat{y}_{,\xi} \\ \hat{x}_{,\eta} & \hat{y}_{,\eta} \end{bmatrix} = \begin{bmatrix} x & 0 \\ 0 & y_{,\eta} \end{bmatrix} = J \tag{3}$$

where J is the Jacobian matrix on boundary.

Using Eqs. (2) and (3), the partial derivations with Cartesian coordinates are expressed as

$$\begin{Bmatrix} \partial/\partial\hat{x} \\ \partial/\partial\hat{y} \end{Bmatrix} = \hat{J}(\xi,\eta)^{-1} \begin{Bmatrix} \partial/\partial\xi \\ \partial/\partial\eta \end{Bmatrix} = \frac{1}{|J|} \begin{Bmatrix} y_{,\eta} \\ 0 \end{Bmatrix} \frac{\partial}{\partial\xi} + \frac{1}{|J|} \begin{Bmatrix} 0 \\ x \end{Bmatrix} \frac{\partial}{\partial\eta} \tag{4}$$

The infinitesimal area S^e in unbound domain is expressed as

$$dS^e = \left|\hat{J}(\xi,\eta)\right| d\xi d\eta = |J| d\xi d\eta \tag{5}$$

2.2 Establishment of the scaled boundary displacement equation

The governing differential equation for the 2D linear elastodynamics in frequency domain is expressed as Eq. (6).

$$L^T \sigma + p + \omega^2 \rho u = 0 \tag{6}$$

with the displacement vector $\{u\}=u(\hat{x}, \hat{y})=[u_x \quad u_y]^T$, the stress vector $\{\sigma\}=[\sigma_x \ \sigma_y \ \tau_{xy}]^T$, and the volume force $\{p\}=[p_x \quad p_y]^T$.

Using Eq. (4), the partial differential operator L is expressed as

$$[L] = \begin{bmatrix} \dfrac{\partial}{\partial \hat{x}} & 0 & \dfrac{\partial}{\partial \hat{y}} \\ 0 & \dfrac{\partial}{\partial \hat{y}} & \dfrac{\partial}{\partial \hat{x}} \end{bmatrix} = [b^1]\dfrac{\partial}{\partial \xi} + [b^2]\dfrac{\partial}{\partial \eta} \tag{7}$$

where $[b^1] = \dfrac{1}{|J|}\begin{bmatrix} y_{,\eta} & 0 \\ 0 & 0 \\ 0 & y_{,\eta} \end{bmatrix}$, $[b^2] = \dfrac{1}{|J|}\begin{bmatrix} 0 & 0 \\ 0 & x \\ x & 0 \end{bmatrix}$.

According to Hooke's law, the relationship between stress and strain is expressed as

$$\{\sigma\} = [D]\{\varepsilon\} \tag{8}$$

where the strain vector $\{\varepsilon\}=[\varepsilon_x \quad \varepsilon_y \quad \gamma_{xy}]^T=[L]\{u\}$, and the elasticity matrix $[D]$.

$\{t^\xi\}$ and $\{t^\eta\}$ are the normal stress vectors of lines S^e and S^η, respectively. They are expressed as

$$\{t^\xi\} = \dfrac{|J|}{g^\xi}[b^1]^T\{\sigma\} \quad , \quad \{t^\eta\} = \dfrac{|J|}{g^\eta}[b^2]^T\{\sigma\} \tag{9}$$

where $g^\xi=y$, $g^\eta=x$.

For $\xi=const$, the infinitesimal arc is expressed as

$$d\Gamma^e = \sqrt{(x_{,\eta})^2 + (y_{,\eta})^2}\,d\xi = \left| y_{,\eta} \right| d\xi \tag{10}$$

The Galerkin's weighted residual method with the scaled boundary coordinates ξ and η is applied to the governing differential Eq. (6).

$$\int_S w^T[b^1]^T\{\sigma\}_{,\xi}dS + \int_S w^T[b^2]^T\{\sigma\}_{,\eta}dS + \omega^2\int_S w^T\rho u(\xi,\eta)dS + \int_S w^T p\,dS = 0 \tag{11}$$

where the weight function $w=w(\xi, \eta)$.

The displacement $\{u\}$ and weight function $\{w\}$ are discretized analogously to the method in Eq. (1)

$$\{u(\xi,\eta)\} = N(\eta)\{u(\xi)\}, \quad \{w(\xi,\eta)\} = N(\eta)\{w(\xi)\} \tag{12}$$

Using Eqs. (7), (8) and (12), the relationship between stress and node displacements is expressed as

$$\{\sigma\} = [D]([b^1]N(\eta)\{u(\xi)\}_{,\xi} + [b^2]N(\eta)_{,\eta}\{u(\xi)\}) = D(B^1\{u(\xi)\}_{,\xi} + B^2\{u(\xi)\}) \tag{13}$$

where

$$[B^1] = [b^1][N(\eta)], \qquad [B^2] = [b^2][N(\eta)]_{,\eta} \tag{14}$$

Hence, the matrices $[B^1]$ and $[B^2]$ represent the stress-node displacement relationship. They only depend on the boundary geometry of the problem domain which is the same as the original SBFEM. According to Eq. (13), the differentiation of stress vector $\{\sigma\}$ with ξ and η are expressed as

$$\{\sigma\}_{,\xi} = [D]([B^1]\{u(\xi)\}_{,\xi\xi} + [B^2]\{u(\xi)\}_{,\xi}) \tag{15a}$$

$$\{\sigma\}_{,\eta} = [D]([b^1][N(\eta)]_{,\eta}\{u(\xi)\}_{,\xi} + [b^2][N(\eta)]_{,\eta\eta}\{u(\xi)\}) \tag{15b}$$

Considering the sun I_1 of the first term of Eq. (11), it is formulated as Eq. (16) by using Eqs. (5) and (12).

$$
\begin{aligned}
I_1 &= \int_S w^T \{b^1\}^T \{\sigma\}_{,\xi} d_S \\
&= \iint w(\xi)^T N(\eta)^T \{b^1\}^T D([B^1]\{u(\xi)\}_{,\xi\xi} + [B^2]\{u(\xi)\}_{,\xi}) |J| d\eta d\xi \\
&= \iint w(\xi)^T [B^1]^T D([B^1]\{u(\xi)\}_{,\xi\xi} + [B^2]\{u(\xi)\}_{,\xi}) |J| d\eta d\xi \\
&= \int w(\xi)^T ([E^0]\{u(\xi)\}_{,\xi\xi} + [E^1]^T \{u(\xi)\}_{,\xi}) d\xi
\end{aligned} \tag{16}
$$

For the sake of simplicity, introducing the coefficient matrices

$$[E^0] = \int_{S^\xi} [B^1]^T [D][B^1] |J| d\eta \tag{17a}$$

$$[E^1] = \int_{S^\xi} [B^2]^T [D][B^1] |J| d\eta , \tag{17b}$$

$$[E^2] = \int_{S^\xi} [B^2]^T [D][B^2] |J| d\eta , \tag{17c}$$

$$[M^0] = \int_{S^\xi} [N]^T \rho [N] |J| d\eta , \tag{17d}$$

The second, third and fourth terms of Eq. (11) sum as I_2, I_3, I_4, respectively. Integrating by parts and using Eqs. (5) and (12), I_2, I_3 and I_4 are expressed as

$$
\begin{aligned}
I_2 &= \iint w(\xi)^T N(\eta)^T \{b^2\}^T [D](\{b^1\}N(\eta)_{,\eta}\{u(\xi)\}_{,\xi} + \{b^2\}N(\eta)_{,\eta\eta}\{u(\xi)\}) |J| d\eta d\xi \\
&= \iint (-w(\xi)^T [B^2]^T [D][B^1]\{u(\xi)\}_{,\xi} - w(\xi)^T [B^2]^T [D][B^2]\{u(\xi)\}) |J| d\eta d\xi \\
&= \int (-w(\xi)^T [E^1]\{u(\xi)\}_{,\xi} - w(\xi)^T [E^2]\{u(\xi)\}) d\xi
\end{aligned} \tag{18}
$$

$$
\begin{aligned}
I_3 &= \int w(\xi)^T \rho d_S = \iint w(\xi)^T N(\eta)^T p |J| d\eta d\xi \\
&= \iint w(\xi)^T N(\eta)^T (\{b^2\}^T \{\sigma\} + p) |J| d\eta d\xi \\
&= \int w(\xi)^T (F^t + F^b) d_\xi \\
&= \int w(\xi)^T F(\xi) d_\xi
\end{aligned} \tag{19}
$$

$$I_4 = \int_S w^T \rho d_S = \iint w(\xi)^T N(\eta)^T \rho \omega^2 N(\eta) u(\xi) |J| d\eta d\xi$$

$$= \int w(\xi)^T \omega^2 M^0 u(\xi) d\xi \tag{20}$$

where $F(\xi) = F^b + F^t$, $F^t = \int_\Gamma N(\eta)^T \{b^2\}^T \{\sigma\} |J| d\xi$, $F^b = \int_{-1}^1 N(\eta)^T p |J| d\eta$.

F^t is the nodal forces resulting from the boundary tractions load, which pass through the scaling line. Because assuming the traction is free at the top of boundary, F^t vanishing. F^b is the nodal forces resulting from the body loads. Eq. (11) can be written as displacement equation as follow

$$[E^0]u(\xi)_{,\xi\xi} + ([E^1]^T - [E^1])u(\xi)_{,\xi} - [E^2]u(\xi) + \omega^2 M^0 u(\xi) + F(\xi) = 0 \tag{21}$$

The modified SBFE equation in displacement for the 2D layered medium is shown in Eq. (21). It is a linear second order differential equation. For the sake of obtaining the dynamic stiffness, it is transformed into an equivalent system of nonlinear first order differential equation in the next section.

2.3 Establishment of the scaled boundary dynamic stiffness equation

Eq. (21) is a linear second order differential equation, it can transform into a one order partial differential equation in dynamic stiffness. Applying the principle of virtual work to the internal nodal forces $\{Q(\xi)\}$ equation, the equation can be expressed as

$$w(\xi)^T \{Q(\xi)\} = \int_\Gamma w(t^\xi)^T \sigma d\Gamma^\xi \tag{22}$$

Substituting Eqs. (9) and (10) into Eq. (22) leads to

$$\{Q(\xi)\} = [E^0]\{u(\xi)\}_{,\xi} + [E^1]^T \{u(\xi)\} \tag{23}$$

For the unbound domain, the relationship between the internal nodal forces $\{Q(\xi)\}$ and the external nodal loads $\{R(\xi)\}$ can be expressed as

$$\{R(\xi)\} = -\{Q(\xi)\} \tag{24}$$

In frequency domain, the relationship between displacement amplitude and external nodal loads can be expressed as

$$\{R(\xi)\} = [S(\omega)]\{u(\xi)\} - R^F(\xi) \tag{25}$$

where the term $\{R^F(\xi)\}$ is the nodal force resulting from surface stresses.

Using Eqs. (23), (24), (25) and then solving $\{u(\xi)\}_{,\xi}$, Eq. (26) is obtained which is differentiated with respect to ξ. Therefore, yields $\{u(\xi)\}_{,\xi\xi}$ (as shown in Eq. (27)).

$$\{u(\xi)\}_{,\xi} = (R^F(\xi) - ([S(\omega)] + [E^1]^T)\{u(\xi)\})[E^0]^{-1} \tag{26}$$

$$\{u(\xi)\}_{,\xi\xi} = (R^F(\xi)_{,\xi} - ([S(\omega)] + [E^1]^T)\{u(\xi)\}_{,\xi})[E^0]^{-1} \tag{27}$$

Substituting Eqs. (26) and (27) into Eq. (21)

$$((([S(\omega)]+[E^1])[E^0]^{-1}([S(\omega)]+[E^1]^T)-[E^2]+$$
$$\omega^2[M^0])\{u(\xi)\}+R^F(\xi)_{,\xi}-([S(\omega)]+[E^1])[E^0]^{-1}R^F(\xi)+F(\xi)=0 \tag{28}$$

For the arbitrary displacements, the coefficient of $\{u(\xi)\}$ term must vanish. Thus, the scaled boundary equation in dynamic stiffness $[S(\omega)]$ is obtained

$$([S(\omega)]+[E^1])[E^0]^{-1}([S(\omega)]+[E^1]^T)-[E^2]+\omega^2[M^0]=0 \tag{29}$$

Eq. (29) is the SBFE dynamic stiffness equation for the 2D unbounded domain on rigid bedrock. It is obviously different from the original SBFE dynamic stiffness equation. The original dynamic stiffness equation (Wolf 2003) is a differential equation with respect to ξ, and it can not be solved directly. However, the Eq. (29) is a standard Riccati equation, and it can be solved directly in frequency domain. For the sake of calculating the time domain problem, the dynamic stiffness is expanded into a series of continued fractions. The detailed process is presented in section 3.

3. Continued fraction solution of dynamic stiffness

The continued fraction derivation process is similar to the method in Reference (Bazyar and Song 2008). Dynamic stiffness is decomposed into a power series in $i\omega$ with decreasing exponent. The high frequency part of dynamic characteristics is modeled. Along with increasing the order of continued fraction, the numerical accuracy increases. The scaled boundary finite element Eq. (29) in dynamic stiffness is written as

$$\left([S(\omega)]+[E^1]\right)[E^0]^{-1}\left([S(\omega)]+[E^1]^T\right)-[E^2]+\omega^2[M^0]=0 \tag{30}$$

Similar Eq. (23) in Reference (Song 2011), the dynamic stiffness $[S(\omega)]$ is expressed as

$$[S(\omega)]=[K]+i\omega[C]-[Y^{(1)}(\omega)] \tag{31}$$

where the terms $[K]$ and $[C]$ are the static stiffness matrix and damping matrix, respectively. The high order expansion term $[Y^{(1)}(\omega)]$ will be introduced in the following steps.

The first two terms are expressed as the low frequency parts of the dynamic stiffness $[S(\omega)]$ which is the same as the finite element method. The remaining term $[Y^{(1)}(\omega)]$ expresses the high frequency part of $[S(\omega)]$. Substituting Eq. (31) into Eq. (30) yields

$$\left([K]+i\omega[C]-[Y^{(1)}(\omega)]+[E^1]\right)[E^0]^{-1}\left([K]+i\omega[C]-[Y^{(1)}(\omega)]+[E^1]^T\right)-[E^2]+\omega^2[M^0]=0 \tag{32}$$

Eq. (32) can be written in ascending order of the power of $i\omega$. It contains a linear term, a quadratic term and higher order residual term, respectively. Setting the coefficient matrix of each term equal to zero, we can obtain the stiffness matrix $[K]$, damping matrix $[C]$ and high order term $[Y^{(1)}(\omega)]$, respectively. The coefficients of the quadratic term and the linear term yield an algebraic Riccati equation for the stiffness matrix and damping matrix, respectively. The two equations are expressed as

$$(i\omega)^2 \ : \ [C][E^0]^{-1}[C]-[M^0]=0 \tag{33}$$

$$i\omega \ : \ [C][E^0]^{-1}[K]+[K][E^0]^{-1}[C]+[C][E^0]^{-1}[E^1]^T+[E^1][E^0]^{-1}[C]=0 \tag{34}$$

Eqs. (33) and (34) are scaled boundary finite element equations of damping matrix $[C]$ and static stiffness matrix $[K]$, respectively. Both of them are algebraic Riccati equations, and the detailed solving process is addressed in References (Song 2004, Laub 1979). The residual term of Eq. (32) is set to zero leading to

$$[Y^{(1)}]^{-1}[E^0]^{-1}[Y^{(1)}]^{-1} - (i\omega[C][E^0]^{-1} + [K][E^0]^{-1} + [E^1][E^0]^{-1})[Y^{(1)}]^{-1} -$$
$$[Y^{(1)}]^{-1}(i\omega[E^0]^{-1}[C] + [E^0]^{-1}[K] + [E^0]^{-1}[E^1]^T) + [K][E^0]^{-1}[K] + [K][E^0]^{-1}[E^1]^T \quad (35)$$
$$+[E^1][E^0]^{-1}[K] + [E^1][E^0]^{-1}[E^1]^T - [E^2] = 0$$

Similar to the dynamic stiffness $[S(\omega)]$, the unknown residual term $[Y^{(1)}(\omega)]$ is expressed as

$$[Y^{(1)}(\omega)] = [Y_0^{(1)}] + i\omega[Y_1^{(1)}] - [Y^{(2)}]^{-1} \quad (36)$$

with $i=1$ and

$$[Y^{(i)}(\omega)] = [Y_0^{i(}] + i\omega[Y_1^{i}] - [Y^{i+}(\omega)] \quad (37)$$

In Eq. (37), $[Y_0^{(i)}]$ is constant term, $[Y_1^{(i)}]$ is linear term, and $[Y^{(i+1)}(\omega)]$ is the high order residual term. The equation for $[Y^{(1)}(\omega)]$ is obtained by pre-multiplying and post-multiplying Eq. (35) by $[Y^{(1)}(\omega)]$, respectively.

$$[E^0]^{-1} - [Y^{(1)}](i\omega[C] + [K] + [E^1])[E^0]^{-1} - [E^0]^{-1}(i\omega[C] + [K] + [E^1]^T)[Y^{(1)}]$$
$$+[Y^{(1)}](([K] + [E^1] + [E^1])[E^0]^{-1}([K] + [E^1]^T) - [E^2])[Y^{(1)}] = 0 \quad (38)$$

Eq. (38) is written as the case $i=1$ of the following equation

$$[a^{(i)}] - [Y^{(1)}](i\omega[b_1^{(1)}]^T + [b_0^{(1)}]^T) - (i\omega[b_1^{(1)}] + [b_0^{(1)}])[Y^{(1)}] + [Y^{(1)}][c^{(1)}][Y^{(1)}] = 0 \quad (39)$$

with the coefficient matrices defined as

$$[a^{(1)}] = [E^0] \quad (40a)$$

$$[b_0^{(1)}] = [E^0]^{-1}([K] + [E^1]^T) \quad (40b)$$

$$[b_1^{(1)}] = [E^0]^{-1}[C] \quad (40c)$$

$$[c^{(1)}] = ([K] + [E^1])[E^0]^{-1}([K] + [E^1]^T) - [E^2] \quad (40d)$$

Substituting Eq. (37) into Eq. (39), and it is expanded in ascending order of the power of $i\omega$ again, as shown in Eq. (41).

$$[a^{(i)}] - ([Y_0^{(i)}] + i\omega[Y_1^{(i)}] - [Y^{(i+1)}]^{-1})(i\omega[b_1^{(i)}]^T + [b_0^{(i)}]^T) -$$
$$(i\omega[b_1^{(i)}] + [b_0^{(i)}])([Y_0^{(i)}] + i\omega[Y_1^{(i)}] - [Y^{(i+1)}]^{-1}) + \quad (41)$$
$$([Y_0^{(i)}] + i\omega[Y_1^{(i)}] - [Y^{(i+1)}]^{-1})[c^i]([Y_0^{(i)}] + i\omega[Y_1^{(i)}] - [Y^{(i+1)}]^{-1}) = 0$$

Setting the coefficient matrix of each term equal to zero leads to

$$(i\omega)^2 \; : \; -[Y_1^{(i)}][b_1^{(i)}]^T - [b_1^{(i)}][Y_1^{(i)}] + [Y_1^{(i)}][c^{(i)}][Y_1^{(i)}] = 0 \quad (42)$$

$$i\omega \; : \; \begin{matrix} [Y_0^{(i)}]([c^{(i)}][Y_1^{(i)}] - [b_1^{(i)}]^T) + ([Y_1^{(i)}][c^{(i)}] - [b_1^{(i)}])[Y_0^{(i)}] - \\ [Y_1^{(i)}][b_0^{(i)}]^T - [b_0^{(i)}][Y_1^{(i)}] = 0 \end{matrix} \quad (43)$$

Eq. (42) is a Lyapunov equation for $[Y_1^{(i)}]$. The solution is described in detail in Reference (Song and Wolf 1997). Eq. (43) is a algebraic Riccati equation, the solving process is the same as $[K]$. Setting the residual term equal to zero, it can be expressed as

$$
\begin{aligned}
&[Y^{(i+1)}]^{-1}[c^{(i)}][Y^{(i+1)}]^{-1} + [Y^{(i+1)}]^{-1}(i\omega([b_1^{(i)}]^T - [c^{(i)}][Y_1^{(i)}]) + [b_0^{(i)}]^T - [c^{(i)}][Y_0^{(i)}]) \\
&+(i\omega([b_1^{(i)}] - [Y_1^{(i)}][c^{(i)}]) + [b_0^{(i)}] - [Y_0^{(i)}][c^{(i)}])[Y^{(i+1)}]^{-1} + \\
&[a^{(i)}] - [Y_0^{(i)}][b_0^{(i)}]^T - [b_0^{(i)}][Y_0^{(i)}] + [Y_0^{(i)}][c^{(i)}][Y_0^{(i)}] = 0
\end{aligned}
\tag{44}
$$

The equation for $[Y^{(i+1)}(\omega)]$ is obtained by pre-multiplying and post-multiplying Eq. (44) by $[Y^{(i+1)}(\omega)]$ and $[Y^{(i+1)}(\omega)]$, respectively, an it can be expressed as

$$
\begin{aligned}
&[c^{(i)}] + (i\omega([b_1^{(i)}]^T - [c^{(i)}][Y_1^{(i)}]) + [b_0^{(i)}]^T - [c^{(i)}][Y_0^{(i)}])[Y^{(i+1)}] + \\
&[Y^{(i+1)}](i\omega([b_1^{(i)}] - [Y_1^{(i)}][c^{(i)}]) + [b_0^{(i)}] - [Y_0^{(i)}][c^{(i)}]) \\
&+[Y^{(i+1)}]([a^{(i)}] - [Y_0^{(i)}][b_0^{(i)}]^T - [b_0^{(i)}][Y_0^{(i)}] + [Y_0^{(i)}][c^{(i)}][Y_0^{(i)}])[Y^{(i+1)}] = 0
\end{aligned}
\tag{45}
$$

Eq. (45) is written as the case $i=i+1$ of the following equation

$$
\begin{aligned}
&[a^{(i+1)}] - [Y^{(i+1)}](i\omega[b_1^{(i+1)}]^T + [b_0^{(i+1)}]^T) - (i\omega[b_1^{(i+1)}] + [b_0^{(i+1)}])[Y^{(i+1)}] \\
&+[Y^{(i+1)}][c^{(i+1)}][Y^{(i+1)}] = 0
\end{aligned}
\tag{46}
$$

where the coefficient matrices defined as

$$
[a^{(i+1)}] = [c^{(i)}]
\tag{47a}
$$

$$
[b_1^{(i+1)}] = [c^{(i)}][Y_1^{(i)}] - [b_1^{(i)}]^T
\tag{47b}
$$

$$
[b_0^{(i+1)}] = [c^{(i)}][Y_0^{(i)}] - [b_0^{(i)}]^T
\tag{47c}
$$

$$
[c^{(i+1)}] = [a^{(i)}] - [Y_0^{(i)}][b_0^{(i)}]^T - [b_0^{(i)}][Y_0^{(i)}] + [Y_0^{(i)}][c^{(i)}][Y_0^{(i)}]
\tag{47d}
$$

Eq. (46) is simply the $i+1$ case of Eq. (39). The coefficient matrices $[a^{(i)}]$, $[b_0^{(i)}]$, $[b_1^{(i)}]$, and $[c^{(i)}]$ for $i \geq 2$ case will be updated by using Eq. (47). Therefore, the solving process can be recursive. It is terminated when i is equal to the order of continued fraction M with the assumption $[Y^{(M+1)}(\omega)]=0$.

4. Time domain solution of the scaled boundary dynamic stiffness equation

4.1 Established bounded domain time-domain motion equation

The bounded domain is modeled by the standard finite element method. Standard isoparametric 8-node plane elements are employed to model the bounded domain. The finite element model can couple with the SBFE model seamlessly by employing compatible shape functions. The equation of motion for bounded domain is expressed as

$$
\begin{bmatrix} M_{ss} & M_{sb} \\ M_{bs} & M_{bb} \end{bmatrix} \begin{Bmatrix} \{\ddot{u}_s\} \\ \{\ddot{u}_b\} \end{Bmatrix} + \begin{bmatrix} K_{ss} & K_{sb} \\ K_{bs} & K_{bb} \end{bmatrix} \begin{Bmatrix} \{u_s\} \\ \{u_b\} \end{Bmatrix} = \begin{Bmatrix} P_s \\ P_b \end{Bmatrix} - \begin{Bmatrix} 0 \\ R_b \end{Bmatrix}
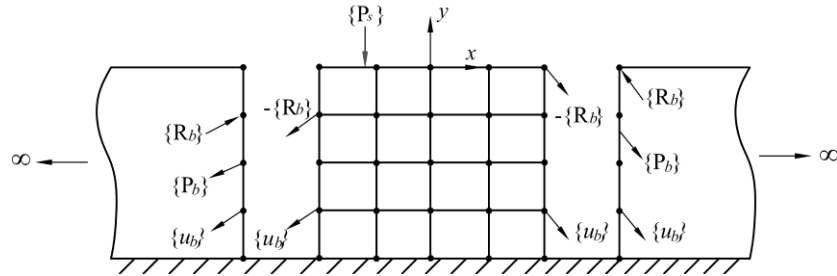\tag{48}
$$

Fig. 2 Coupled model of finite element method and scaled boundary finite element method

where the subscript s expresses the freedom degrees which only belong to the bounded domain. Subscript b expresses the freedom degrees of interface. As shown in Fig. 2, interaction forces $[R_b]$ act on the boundary of bounded domain/unbounded domain. External forces $\{P_s\}$ act on the bounded domain. $\{\ddot{u}\}$ and $\{u\}$ are velocity and acceleration, respectively. Eq. (48) is simplified into Eq. (49). The Eq. (49) is the bounded domain equation of motion in time domain.

$$[M]_b\{\ddot{u}(t)\}+[K]_b\{u(t)\}=\{f(t)\}_b \tag{49}$$

4.2 Established unbounded domain time-domain motion equation

The dynamic stiffness matrix is expanded to a series of continued fraction forms. Introducing auxiliary variables, the equations of motion are obtained. The detailed process is analogous to Reference (Chen and Du 2014). Therefore, the purpose of this section is transformation the frequency domain solution of the unbounded domain into the time domain solution.

Substituting Eq. (31) into the force displacement relationship (Eq. (25)), it is expressed as

$$\{R(\omega)\}=([K]+i\omega[C])\{u(\omega)\}-i\omega\{u^{(1)}(\omega)\} \tag{50}$$

where the virtual auxiliary variable $\{u^{(1)}(\omega)\}$ is defined as

$$\{u(\omega)\}=[Y^{(1)}(x)]\{u^{(1)}(\omega)\} \tag{51}$$

Eq. (51) is for $i=1$ case, when $i>1$ Eq. (51) transforms into the following form

$$\{u^{(i-1)}(\omega)\}=[Y^{(i)}(\omega)]\{u^{(i)}(\omega)\} \tag{52}$$

where $\{u^{(0)}(\omega)\}=\{u(\omega)\}$. The $[Y^{(i)}(\omega)]$ is decomposed into a constant term, a linear term and a high order term in Eq. (37). Holding on the constant term and linear term, they are substituted into Eq. (52)

$$\{u^{(i-1)}(\omega)\}=([Y_0^{(i)}]+i\omega[Y_1^{(i)}])\{u^{(i)}(\omega)\}-i\omega\{u^{(i+1)}(\omega)\} \tag{53}$$

Similarly as Eq. (51), $\{u^{(i+1)}(\omega)\}$ is the $i+1$ order auxiliary variable. It is assumed negligible. Combining Eqs. (50) and (53), the equation of motion can be expressed as

$$([K_u]+i\omega[C_u])\{u(\omega)\}=\{F(\omega)\} \tag{54}$$

where

$$
[K_u] = \begin{bmatrix}
[K] & -[I] \\
-[I] & [Y_{0\_r}^{(1)}] & -[I] \\
 & -[I] & [Y_{0\_r}^{(2)}] \\
 & & & \ddots & -[I] \\
 & & & -[I] & [Y_{0\_r}^{(M-1)}] & -[I] \\
 & & & & -[I] & [Y_{0\_r}^{(M)}] & -[I] \\
 & & & & & -[I] & [Y_{0\_l}^{(1)}] & -[I] \\
 & & & & & & -[I] & [Y_{0\_l}^{(2)}] \\
 & & & & & & & & \ddots & -[I] \\
 & & & & & & & & -[I] & [Y_{0\_l}^{(M-1)}] & -[I] \\
 & & & & & & & & & -[I] & [Y_{0\_l}^{(M)}]
\end{bmatrix} \tag{55a}
$$

$$
[C_u] = \begin{bmatrix}
[C] \\
 & [Y_{1\_r}^{(1)}] \\
 & & [Y_{1\_r}^{(2)}] \\
 & & & \ddots \\
 & & & & [Y_{1\_r}^{(M-1)}] \\
 & & & & & [Y_{1\_r}^{(M)}] \\
 & & & & & & [Y_{1\_l}^{(1)}] \\
 & & & & & & & [Y_{1\_l}^{(2)}] \\
 & & & & & & & & \ddots \\
 & & & & & & & & & [Y_{1\_l}^{(M-1)}] \\
 & & & & & & & & & & [Y_{1\_l}^{(M)}]
\end{bmatrix} \tag{55b}
$$

In Eq. (55), $[K]$ is the static stiffness matrix, $[C]$ is the damping matrix, $[I]$ is the unit matrix. $[K_u]$ and $[C_u]$ can be approximated as the high order static stiffness matrix and mass matrix, respectively. Due to the matrices $[K]$, $[C]$, $[Y_0]$ and $[Y_1]$ are symmetric. The block matrices $[K_u]$ and $[C_u]$ are both symmetric and sparse. Subscripts l and r represent the left and the right side of unbounded domain, respectively. Eq. (54) can be expressed into the equation of motion in time domain as

$$
[K_u]\{u(t)\} + [C_u]\{\dot{u}(t)\} = \{f(t)\}_u \tag{54}
$$

5. Coupled bounded and unbounded domain

By means of the interaction force $[R_b]$ on the interface, the bounded domain can be coupled with the unbounded domain. As both the Eqs. (49) and (54) are with respect to $\{u(t)\}$, the seamless coupling can be realized if only the same shape functions are applied in bounded and unbounded domain. For the linear system, the coupled equation of motion can be obtained by combining Eqs. (49) and (54) in time domain. The global equation of motion is expressed as

$$
[K_c]\{u_c\} + [C_c]\{\dot{u}_c\} + [M_c]\{\ddot{u}_c\} = \{f_c\} \tag{55}
$$

where the global coefficient matrixes $[K_c]$, $[C_c]$, $[M_c]$ and displacement vector $\{u_c\}$, external force vector $\{f_c\}$ are expressed as following

$$[K_c]=\begin{bmatrix}
[K_{ss}] & [K_{sb}] \\
[K_{bs}] & [K_{bb}]+[K_\infty] & -[I] \\
& -[I] & [Y_{0\_r}^{(1)}] & -[I] \\
& & -[I] & [Y_{0\_r}^{(2)}] \\
& & & & \ddots & -[I] \\
& & & & -[I] & [Y_{0\_r}^{(M-1)}] & -[I] \\
& & & & & -[I] & [Y_{0\_r}^{(M)}] & -[I] \\
& & & & & & -[I] & [Y_{0\_l}^{(1)}] & -[I] \\
& & & & & & & -[I] & [Y_{0\_l}^{(2)}] \\
& & & & & & & & \ddots & -[I] \\
& & & & & & & & -[I] & [Y_{0\_l}^{(M-1)}] & -[I] \\
& & & & & & & & & -[I] & [Y_{0\_l}^{(M)}]
\end{bmatrix} \tag{56a}$$

$$[M_c]=\begin{bmatrix}
[M_{ss}] & [M_{sb}] \\
[M_{bs}] & [M_{bb}] \\
& & [0] \\
& & & [0] \\
& & & & \ddots \\
& & & & & [0] \\
& & & & & & [0] \\
& & & & & & & [0] \\
& & & & & & & & [0] \\
& & & & & & & & & \ddots \\
& & & & & & & & & & [0] \\
& & & & & & & & & & & [0]
\end{bmatrix} \tag{56b}$$

$$[C_c]=\begin{bmatrix}
[0] & [0] \\
[0] & [C_\infty] \\
& & [Y_{1\_r}^{(1)}] \\
& & & [Y_{1\_r}^{(2)}] \\
& & & & \ddots \\
& & & & & [Y_{1\_r}^{(M-1)}] \\
& & & & & & [Y_{1\_r}^{(M)}] \\
& & & & & & & [Y_{1\_l}^{(1)}] \\
& & & & & & & & [Y_{1\_l}^{(2)}] \\
& & & & & & & & & \ddots \\
& & & & & & & & & & [Y_{1\_l}^{(M-1)}] \\
& & & & & & & & & & & [Y_{1\_l}^{(M)}]
\end{bmatrix} \tag{56c}$$

$$\{u_c\}^T = \left(\{u_s\}^T, \{u_b\}^T, \{u^{(1)}\}^T, \ \{u^{(2)}\}^T, \cdots, \{u^{(M-1)}\}^T, \ \{u^{(M)}\}^T, \{u^{(1)}\}^T, \ \{u^{(2)}\}^T, \cdots, \{u^{(M-1)}\}^T, \ \{u^{(M)}\}^T\right)$$

$$\text{(56d)}$$

$$\{f_c\}^T = \left(\{P_s\}^T, \{P_b\}^T, \{0\}^T, \ \{0\}^T, \cdots, \{0\}^T, \ \{0\}^T, \{0\}^T, \ \{0\}^T, \cdots, \{0\}^T, \ \{0\}^T\right) \qquad \text{(56e)}$$

Eq. (55) is coupled equation of the bounded and unbounded domain in the time domain. It is a second order ordinary differential equation in displacements. Therefore, it can be transformed into an equivalent first order ordinary differential equation as Eq. (57). It is a standard equation of motion with symmetric and sparse coefficient matrices in time domain, and it can be solved by direct integral method (Trinks 2004). This integral method can calculate large number of internal variables at each time step. The computation linearly increases with the order of equation. The efficiency of calculation is greatly improved by this integral method.

$$[K_g]\{z_g\} + [C_g]\{\dot{z}_g\} = \{P_g\} \qquad \text{(57)}$$

where the global stiffness matrix $[K_g]$, the global damping matrix $[C_g]$, the unknown vector $\{z_g\}$, and the force vector $\{P_g\}$ are expresses as

$$[K_g] = \begin{bmatrix}
-[M_{ss}] & -[M_{sb}] \\
-[M_{bs}] & -[M_{bb}] \\
 & & [K_{ss}] & [K_{sb}] \\
 & & [K_{bs}] & [K_{bb}]+[K_\infty] & -[I] \\
 & & & -[I] & [Y_{0\_r}^{(1)}] & -[I] \\
 & & & & -[I] & [Y_{0\_r}^{(2)}] \\
 & & & & & & \ddots & -[I] \\
 & & & & & & -[I] & [Y_{0\_r}^{(M-1)}] & -[I] \\
 & & & & & & & -[I] & [Y_{0\_r}^{(M)}] & -[I] \\
 & & & & & & & & -[I] & [Y_{0\_l}^{(1)}] & -[I] \\
 & & & & & & & & & -[I] & [Y_{0\_l}^{(2)}] \\
 & & & & & & & & & & & \ddots & -[I] \\
 & & & & & & & & & & & -[I] & [Y_{0\_l}^{(M-1)}] & -[I] \\
 & & & & & & & & & & & & -[I] & [Y_{0\_l}^{(M)}]
\end{bmatrix}$$

$$\text{(58a)}$$

$$[C_g] = \begin{bmatrix}
[0] & [0] & [M_{ss}] & [M_{sb}] \\
[0] & [0] & [M_{bs}] & [M_{bb}] \\
[M_{ss}] & [M_{sb}] & [0] & [0] \\
[M_{bs}] & [M_{bb}] & [0] & [C_\infty] \\
 & & & & [Y_{1\_r}^{(1)}] \\
 & & & & & [Y_{1\_r}^{(2)}] \\
 & & & & & & \ddots \\
 & & & & & & & [Y_{1\_r}^{(M-1)}] \\
 & & & & & & & & [Y_{1\_r}^{(M)}] \\
 & & & & & & & & & [Y_{1\_l}^{(1)}] \\
 & & & & & & & & & & [Y_{1\_l}^{(2)}] \\
 & & & & & & & & & & & \ddots \\
 & & & & & & & & & & & & [Y_{1\_l}^{(M-1)}] \\
 & & & & & & & & & & & & & [Y_{1\_l}^{(M)}]
\end{bmatrix}$$

$$\text{(58b)}$$

$$\{p_g\}^T = \left(\{0\}^T, \{0\}^T, \{P_s(t)\}^T, \ \{P_b(t)\}^T, \cdots, \{0\}^T, \ \{0\}^T, \{0\}^T, \ \{0\}^T, \cdots, \{0\}^T, \ \{0\}^T\right) \quad (58c)$$

$$\{z_g\}^T = \begin{pmatrix} \{v_1\}^T, \{v_2\}^T, \{u_s\}^T, \ \{u_b\}^T, \{u^{(1)}\}^T, \{u^{(2)}\}^T, \cdots, \\ \{u^{(M-1)}\}^T, \ \{u^{(M)}\}^T, \{u^{(1)}\}^T, \{u^{(2)}\}^T, \cdots, \{u^{(M-1)}\}^T, \ \{u^{(M)}\}^T \end{pmatrix} \quad (58d)$$

in Eq. (58d)

$$\{v_1\} = \{\dot{u}_s\} \quad (59a)$$

$$\{v_2\} = \{\dot{u}_b\} \quad (59b)$$

The sizes of coefficient matrices $[K_g]$ and $[C_g]$ are $(2N+M_n)\times(2N+M_n)$. M is the order of continued fraction, N is the bounded and unbounded domain total number of degrees of freedom, n is the interface degrees of freedom. Because the coefficient matrices $[K_g]$ and $[C_g]$ are symmetrical and sparse, the computation linearly increases as the order M increases. The stability of the coupled Eq. (57) can not be guaranteed at first. The mainly reason is existing spurious modes in the following eigenvalue problem

$$([K_g] + \lambda[C_g])\{z_g\} = 0 \quad (60)$$

The spurious modes will vanish when the real part of eigenvalue λ is negative or zero. This process is achieved by spectral shifting technique method in Reference (Genes 2012). This guarantees the existence of stable solution.

6. Numerical examples

In this section, numerical examples are produced to verify the accuracy of the modified scaling boundary method in time domain. The effects of the number of layers, soil properties, force form, the soft soil layer on the dynamic response are analyzed in the following. In order to demonstrate the accuracy and advantages of the proposed method, the viscous-spring boundary solution (Deeks and Randolph 1994, Liu *et al.* 2006) is used as the reference solution. In section 6.1, a single layer underlain by the rigid bedrock example is analyzed in time domain. The accuracy of the continued fraction solution by the modified SBFEM is demonstrated. In section 6.2, the two layers model is addressed by comparing the reference solution. In section 6.3, the soft soil layer is considered in a three layers model. The influence of soft soil layer on dynamic response is discussed. In section 6.4, the influences of material parameters are considered. Basing on the control variate method, the influences of shear modulus ratio and the mass density ratio are analyzed, respectively. Finally, the different load forms are compared in section 6.5.

6.1 A single layered medium underlain by rigid bedrock

The dynamic response of a single soil layer with the rigid bedrock is analyzed in this section. As shown in Fig. 3, the thickness of soil layer is defined as $b=1$, the width of bounded domain is defined as $r(r=3b)$. The soil properties are as following, shear modulus $G=1$, Poisson's ratio $v=0.33$ and mass density $\rho=1$. Plane strain state is considered. As shown in Fig. 3, a vertical Ricker wavelet force pulse $P(t)$ which is revealed in Fig. 4 acts on point A. Expression of the force in time and frequency domain are as follow
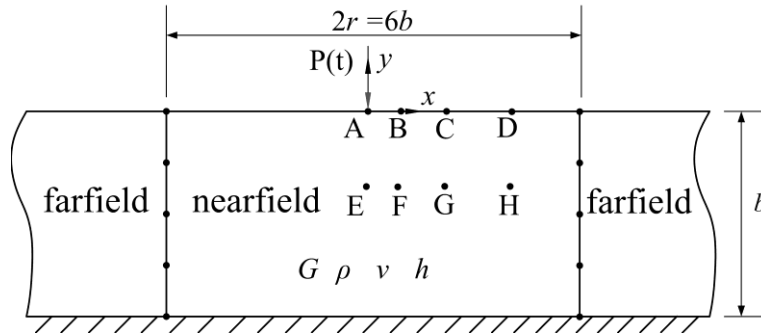
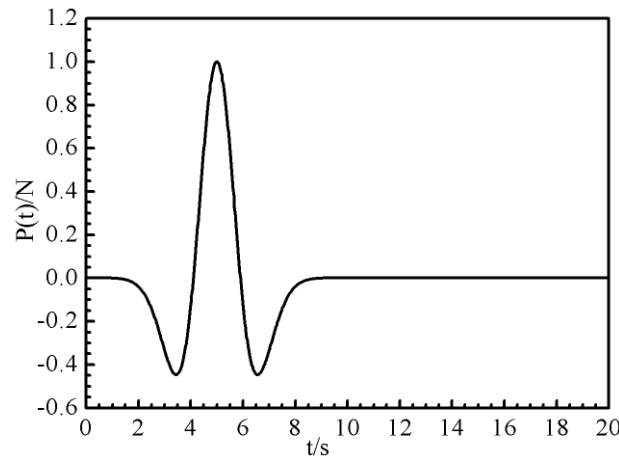Fig. 3 Calculation diagram of one layer model

Fig. 4 Force history of Ricker wavelet

$$P(\text{t}) = P_0\left(1 - 2\left(\frac{t - t_s}{t_0}\right)^2\right)\exp\left(-\left(\frac{t - t_s}{t_0}\right)^2\right) \tag{61a}$$

$$P(\omega) = 0.5\sqrt{\pi}P_0 t_0 (\omega t_0)^2 e^{-0.25(\omega t_0)^2} \tag{61b}$$

where $t_s=5$, $t_0=4/\pi$, $P_0=1$

The single soil layers model is divided into near field and far field. The scaling line of the unbounded domain is located at line OO' as shown in Fig. 1(b). The far field is discretized by 12 three-node elements. It is modeled by using the proposed continued fraction method in time domain with high order stiffness matrix and mass matrix. The order of continued fraction is chosen as $M=8$. The vertical displacements are obtained by solving Eq. (60) using the direct integral method. The time step Δt is chosen as 0.02s with considering 1000 time steps. The near field is analyzed by using the finite element method (Song and Bazyar 2007). It is discretized with 216 eight-node elements, yielding 733 nodes.

In order to demonstrate the accuracy of the proposed method, the viscous-spring boundary coupled with finite element method is introduced to absorb outgoing waves on the boundary. The
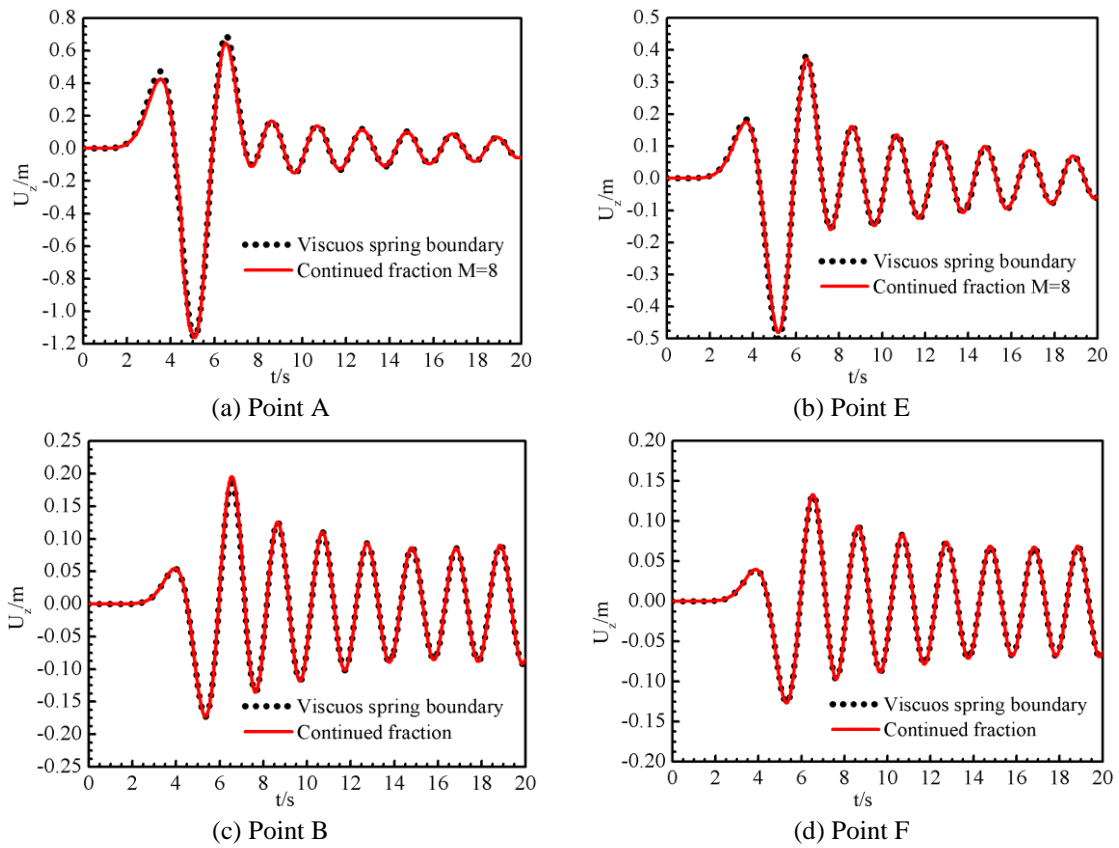
(a) model one   (b) model two
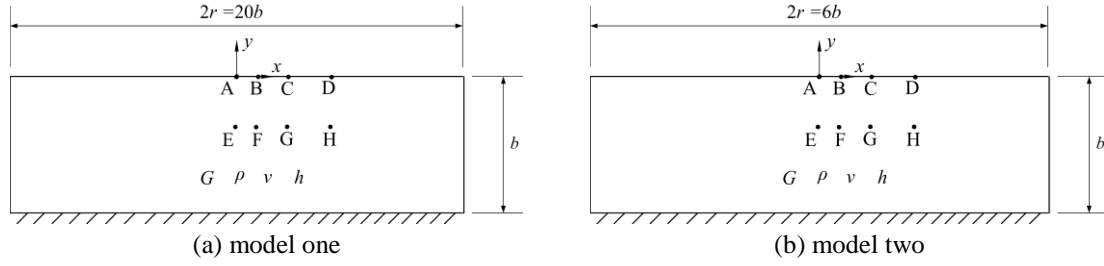
Fig. 5 Viscous-spring boundary model with different *r* values

(a) Point A   (b) Point E

(c) Point B   (d) Point F

Fig. 6 Vertical displacement of observation points in single layered model

viscous-spring boundary is composed of normal and shear directions spring dashpot systems. The spring and damping coefficients (Deeks and Randolph 1994) are expressed as

$$[K_{BN}] = A\frac{G}{r_b}, \quad [C_{BN}] = A\rho c_p \tag{62a}$$

$$[K_{BT}] = A\frac{G}{2r_b}, \quad [C_{BT}] = A\rho c_s \tag{62b}$$

(a) Point A   (b) Point E
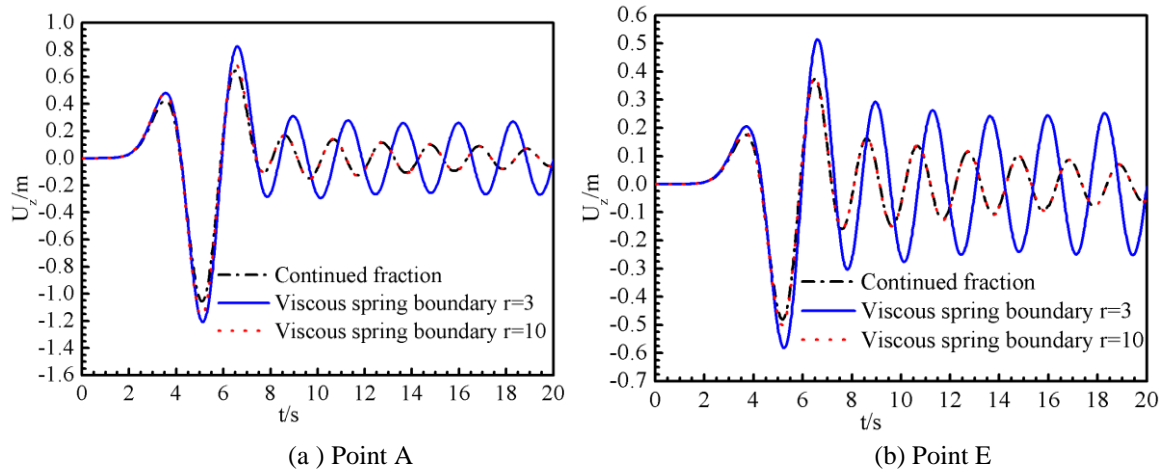
Fig. 7 Vertical displacement of observation points with different *r* value

where the subscripts N and T represent the normal and shear directions, respectively. A is area of the area of problem domain. c_p and c_s are shear wave velocity and P-wave velocity, respectively. G and ρ are defined as shear modulus and mass density, respectively. The r_b is defined as the distance between scattering wave source and the artificial boundary. The viscous-spring boundary solution is used as a reference solution. The finite element model with viscous-spring boundary is discretized with 2040 eight-node elements, yielding 6461 nodes. The physical dimension of model as follows, the thickness of soil layer is defined as b_1 ($b_1=b=1$), and the width is defined as 2_{r1} ($r_1=10$), as shown in Fig. 5(a).

The vertical displacements responses at points A and E are evaluated and compared to the viscous-spring boundary solutions with respect to accuracy in Fig. 6. For time less than about 2.0s, there is a little inconformity but the error is less than 0.05 and can be accepted. This difference is gradually weakened as the time increase. The displacement amplitude increases with increase of the peak value $P(t)$. When $t>8$s, the displacement amplitude is gradually weakened as the time increases. This is because the energy decays when the force tends to zero. It is evident from Fig. 6 that the vertical displacements computing by the proposed method agree very well with the viscous-spring boundary solution for the other time. It is clearly shown that the newly developed continued fraction solution should be very valid.

To illustrate further the correctness of the proposed method, different finite element models with viscous-spring boundary are compared with the solutions of the proposed method. Here, introducing a new finite element model (as shown in Fig. 5(b)), the physical dimension of it is as follows, the thickness of soil layer is defined as b_2 ($b_2=b=1$), and the width is defined as 2_{r2} ($r_2=3b$). It is can be seen from Fig. 7 that the solutions obtaining by the proposed method excellently agree with the reference solutions with width $r_1=10$. It illustrates that the reference solutions with width $r_2=3b$ do not agree with the continued fraction solution and the reference solutions with width $r_1=10$. It is noted that there is oscillatory behavior in Fig. 7. When $0<t<7s$, the reference solution with width $r_2=3b$ vibrates around the continued fraction solutions and the reference solutions with width $r_1=10$. It is noted that the oscillatory behavior of reference solution with width $r_2=3b$ becomes more significant as the time increases. As is known to all, the bigger radiation radius the accuracy of the results is higher. So the displacement results of model one is

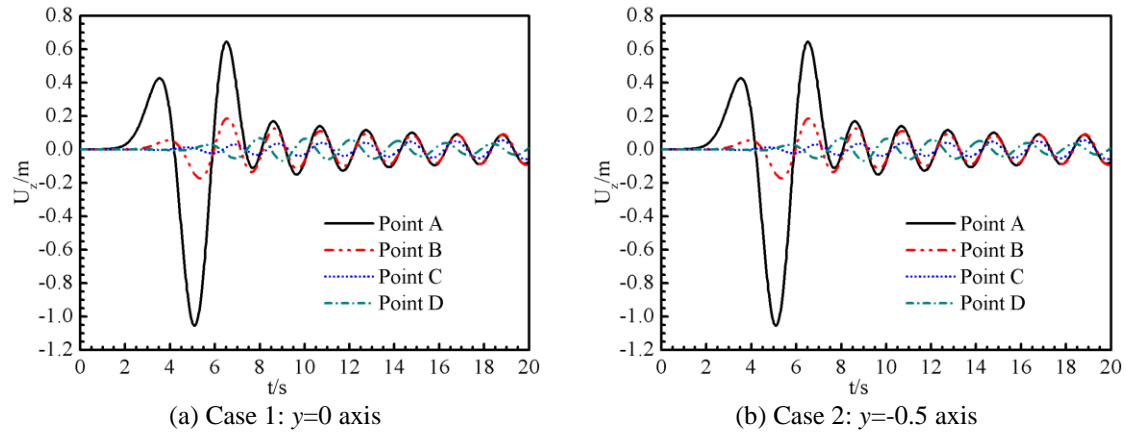(a) Case 1: *y*=0 axis   (b) Case 2: *y*=-0.5 axis

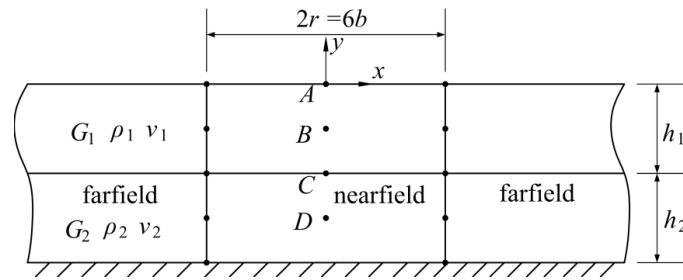Fig. 8 Influence of horizontal distance on the vertical displacements of observation points

Fig. 9 Calculation diagram of two layers model

better than that of model two. The vertical displacements solving by the proposed method agree very well with the reference solution with the radiation radius $r_1=10b$. All of the above show that the proposed method has high precision and it can correctly solve the problem by less degrees of freedom.

In order to illustrate the influence of the horizontal distance on vertical displacement, two cases are introduced. Case 1: Four observant points $A(0,0)$, $B(0.5,0)$, $C(1,0)$ and $D(2,0)$ on the $y=0$ axis are shown in Fig. 3. Case 2: The other four observant points $E(0,-0.5)$, $F(0.5,-0.5)$, $G(1,-0.5)$ and $H(2,-0.5)$ on the $y=-0.5$ axis are also shown in Fig. 3. The vertical displacement responses of them are plotted in Fig. 8. As shown in these two figures, the horizontal distance has greatly influence on the vertical displacement. The vertical displacements generally decrease with the increase of horizontal distances.

6.2 Multi-layered medium underlain by rigid bedrock

To illustrate the proposed method with wide applicability, two numeral examples are presented in sections 6.2.1 and 6.2.2. In this section only the number of layers and soil properties changed, the other parameters are the same as the model in section 6.1.

6.2.1 Two layered medium underlain by rigid bedrock
A two layered medium with the rigid bedrock is shown in Fig. 9. The physical dimension of the

model is indicated in the figure. The layered medium consists of two different materials, and the soil properties are described as follows: shear modulus ratio G_1:G_2=1:0.9, mass density ratio ρ_1:ρ_2=1:0.89 and Poisson's ratio υ_1:υ_2=0.33:0.3. The ratio of layer thickness is h_1:h_2=1:1 and the total soil thickness is b=1. The width of bounded domain is $2r$=6b. Four observation points are selected as: A(0,0), B(0,-0.25), C(0,-0.5), D(0,-0.75). As mentioned in Fig. 4, the Ricker vertical wavelet concentrated force is acted on point A in vertical downward direction.

The continued fraction solutions are compared with the reference solutions in Fig. 10. There is slight difference between the two solutions for the time 5.5<t<6s. However, we can see from those Fig. 10 that the excellent agreements are observed in the other time steps. The results reveal that the continued fraction solutions are suitable to model the multi-layered medium. Comparing with the finite element method, the modified SBFEM in time domain can be applied in many other multi-layered infinite mediums. It evaluates that the proposed method has more generality in solving the time problems.

6.2.2 Three layered medium underlain by rigid bedrock

A three layered medium with the rigid bedrock is shown in Fig.11. The physical dimension of the model is indicated in the figure. The layered medium consists of three different materials, and

(a) Point A

(b) Point B

(c) Point C

(d) Point D
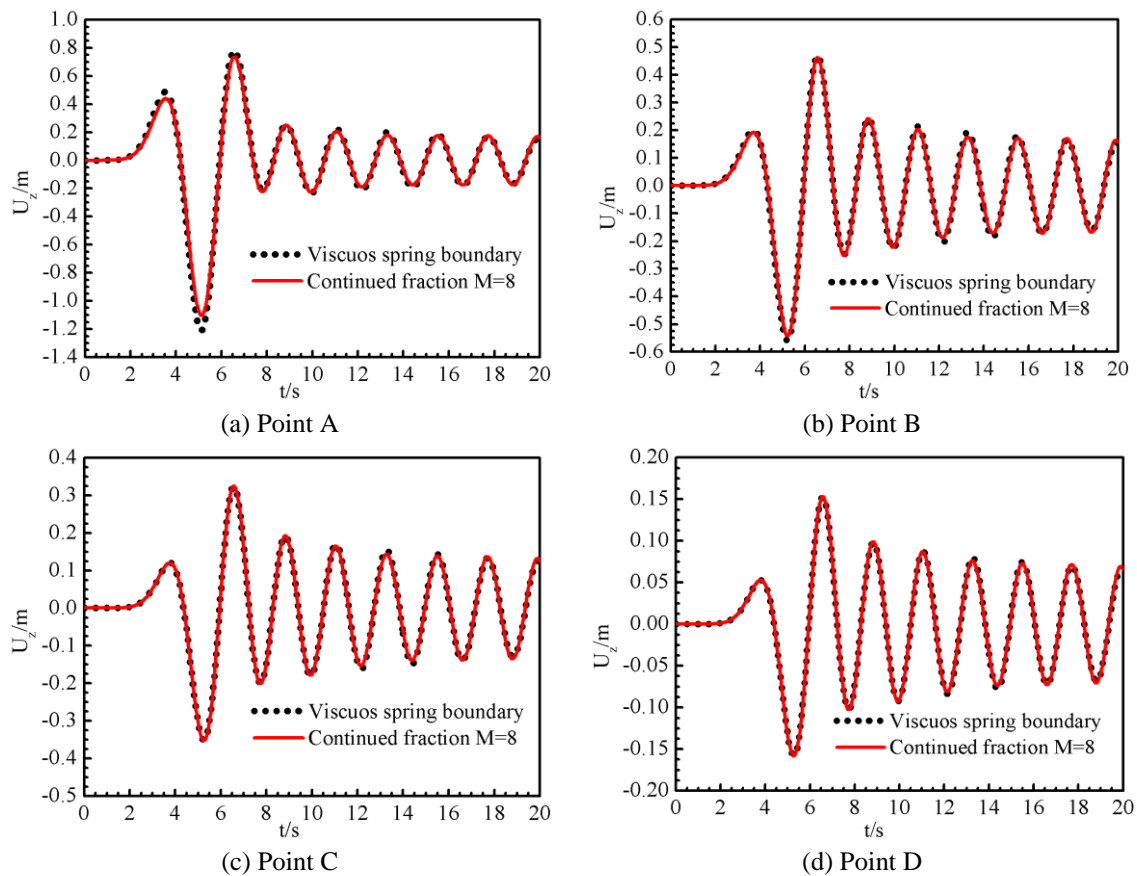
Fig. 10 Vertical displacement of observation points in two layered model.

Fig. 11 Calculation diagram of three layers model

(a) Point A

(b) Point B

(c) Point C
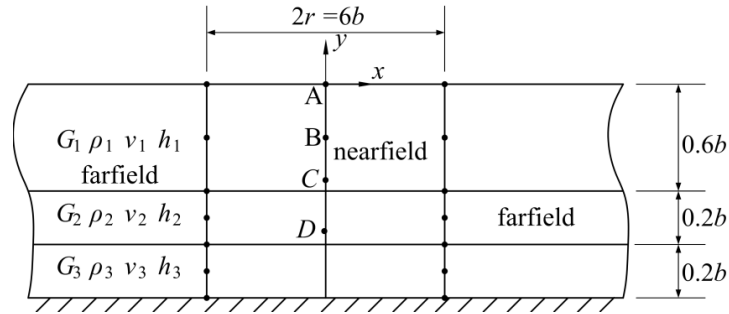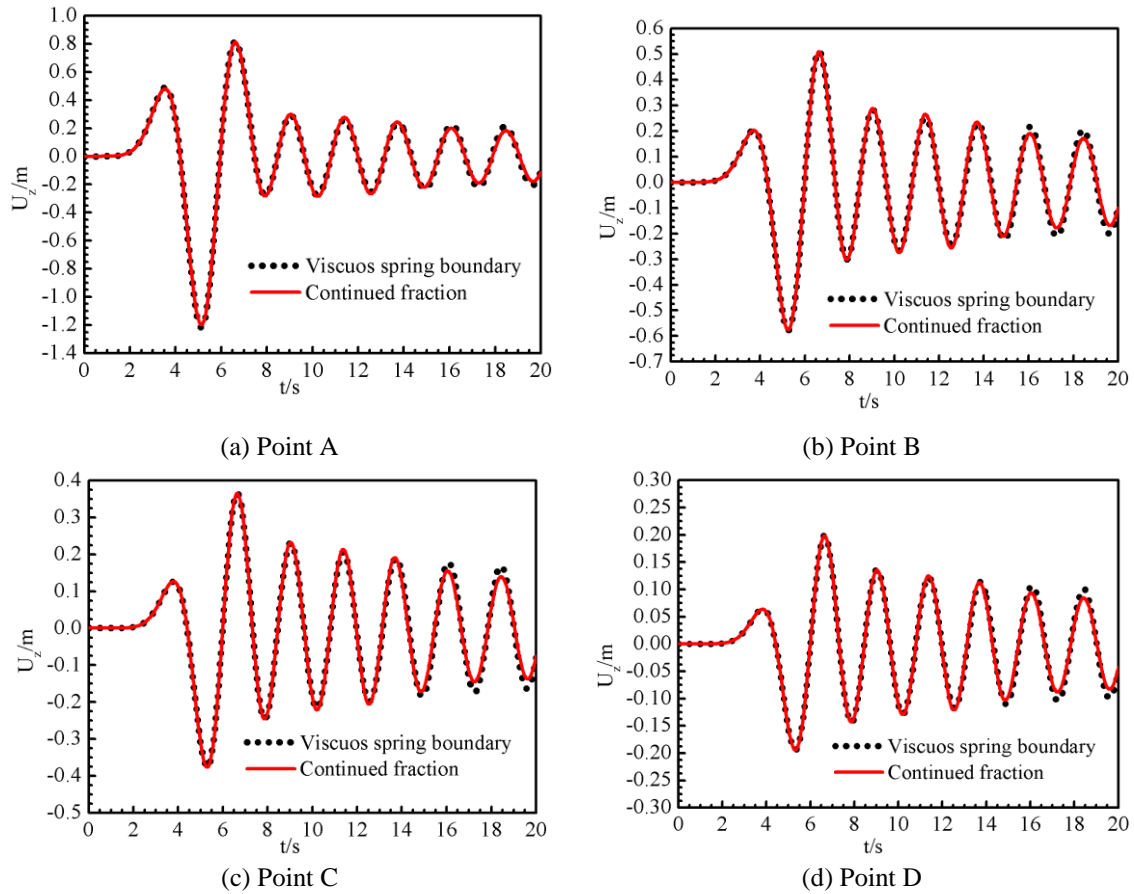
(d) Point D

Fig. 12 Vertical displacement of observation points in three layered model

the soil properties are described as follows: shear modulus ratio $G_1:G_2:G_3$=1:0.9:0.8, mass density ratio $\rho_1:\rho_2:\rho_3$=1:1:0.89 and Poisson's ratio $v_1:v_2:v_3$=0.33:0.3:0.25. The ratio of layer thickness is $h_1:h_2:h_3$=3:1:1 and the total soil thickness is b=1. The width of bounded domain is $2r$=6b. The acting force and position are the same as that of section 6.2.1. Four observation points are selected as: A(0,0), B(0,-0.25), C(0,-0.5), D(0,-0.75).

Table 1 Material properties of the three layers model

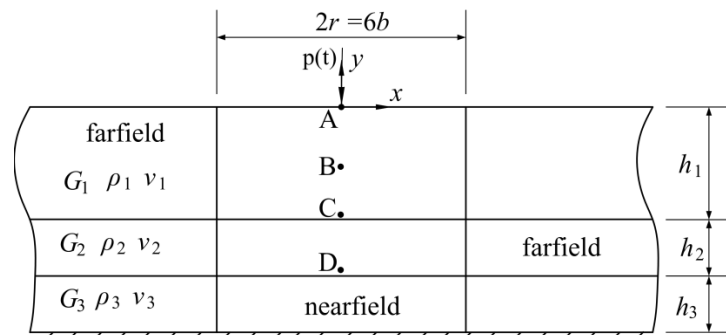| number of soil layer	h	G	ρ	v
1	1/6	0.5	1750	0.25
2	1/3	1.0	1775	0.30
3	1/2	1.5	2050	0.33

Fig. 13 Calculation diagram of three layers model with weak layer

As shown in Fig. 12, it clearly shown that there is a very good agreement between the viscous-spring boundary solutions and the results obtained using the continued fraction method. The number of degrees of freedom in the modified SBFEM is $N_1=2200$, and the number of degrees of freedom in finite element method is $N_2=12216$. The results show that the proposed method using more less degrees of freedom can obtained the same precision as the finite element method. That is, the continued fraction method can obtained accurate solution even for the relatively coarse mesh.

6.3 Influence of soft soil layer on dynamic response.

In order to illustrate the influence of soft soil layer, a three layers soil model is proposed in Fig. 13. The material parameters and layer thickness are listed in Table 1. Layer one is the weak soil layer. Layer two and layer three are the normal soil layer. For the sake of comparing the influence of soft soil layer on dynamic response, the layers are arranged from free face to bottom as follow, case 1: layer one, layer two, layer three; case 2: layer two, layer one, layer three; case 3: layer two, layer three, layer one. The width of bounded domain $2r=6b$ (the total soil layer thickness $b=1$). Four observation points are selected as: $A(0,0)$, $B(0,-0.25)$, $C(0,-0.5)$, $D(0,-0.75)$. The Ricker wavelet impulse which is exhibited in Fig. 4 acts on observation point A.

The changes of the vertical displacements with different cases are presented in Fig. 14. Because the loading point is the surface point, the vertical displacement amplitudes decrease with the depth of observation point increasing and the amplitude of case 1 in Fig. 14(a) is bigger than the other two cases. Comparing Fig. 14(a)-(d), it can be noted that the reflected wave phenomenon is Obviously for $t>7.0s$. Meanwhile, the vertical displacement amplitudes of case 3 are bigger than the other two cases. The amplitudes decreased with the depth of weak layer increasing. The mainly reason is that the weak layer can absorb more energy. And this phenomenon is more obvious with the distance between the loading point and the weak layer decreasing. It is interesting to note that

(a) Point A

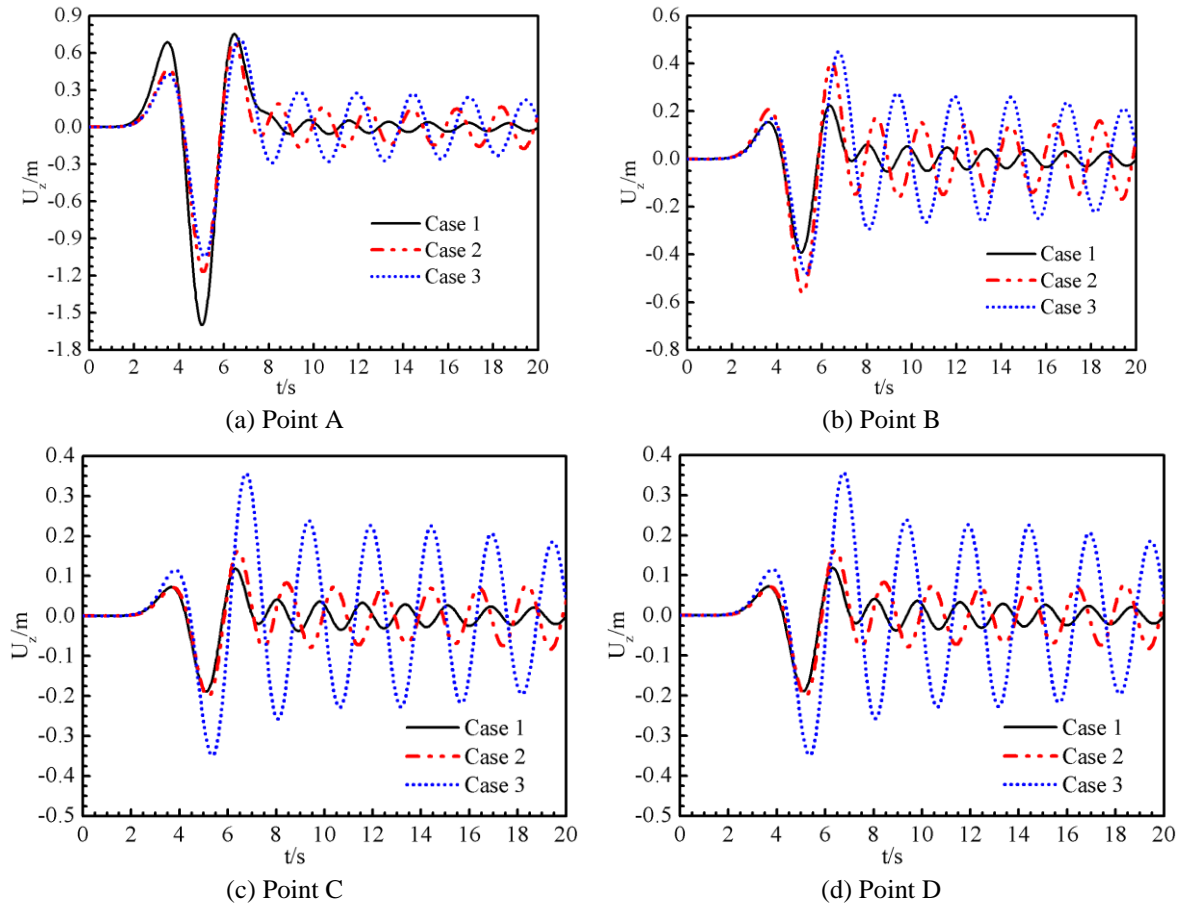(b) Point B

(c) Point C

(d) Point D

Fig. 14 Vertical displacements of observation points in different weak soil layer model

the depth of weak layer plays an important role in dynamic analysis layered model with the weak layer.

6.4 Influence of material parameters on dynamic response.

In the city rail transit, tunnel often runs through the layered soil. The influence of material parameters is more obvious in traffic network. As shown in Fig. 15(a), a two layered model with a tunnel is proposed. The thickness of each layer is equal to $0.5b$ (the total thickness of the soil model $b=1$.). The buried depths of the tunnel $h_1=1/3$, $h_2=5/6$. The width of bounded domain is $2r=6b$. Detailed geometrical dimensions of the tunnel can refer to Fig. 15(b). Six observation points are selected as: $A(0,0)$, $B(0,-0.333)$, $C(0,-0.833)$, $D(0.5,0)$, $E(1,0)$, $F(1.5,0)$, $G(2,0)$. The Ricker wavelet impulse which is exhibited in Fig. 4 acts on observation point A.

In order to consider the influence of the variety of material parameters, the shear modulus and mass density are selected as the variable quantity, respectively. Basing on the control variate method, three cases with various shear modulus are discussed as follow, case 1: $G_1=1$, $G_2=2$; case 2: $G_1=1$, $G_2=1$; case 3: $G_1=1$, $G_2=0.5$.The shear modulus ratio $n=G_1/G_2$ is equal to 0.5, 1.0, 2.0 for
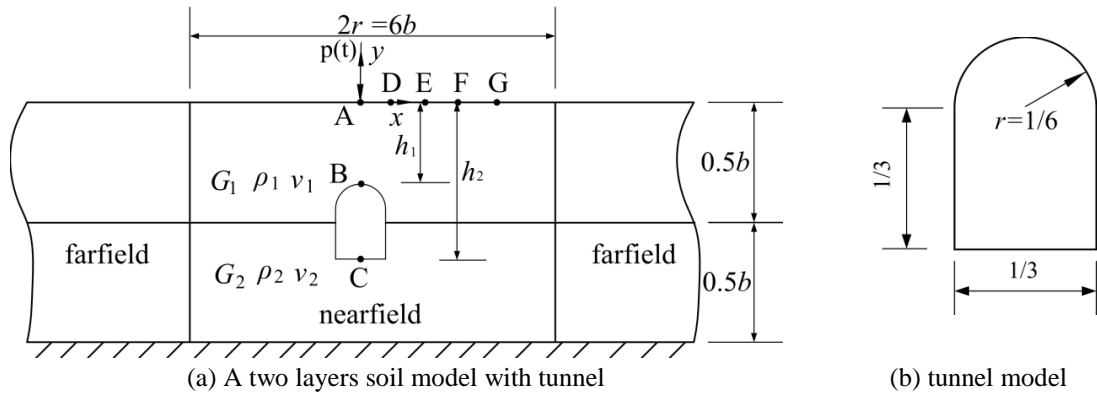
(a) A two layers soil model with tunnel   (b) tunnel model

Fig. 15 Physical dimension of tunnel model

(a) Point A   (b) Point B
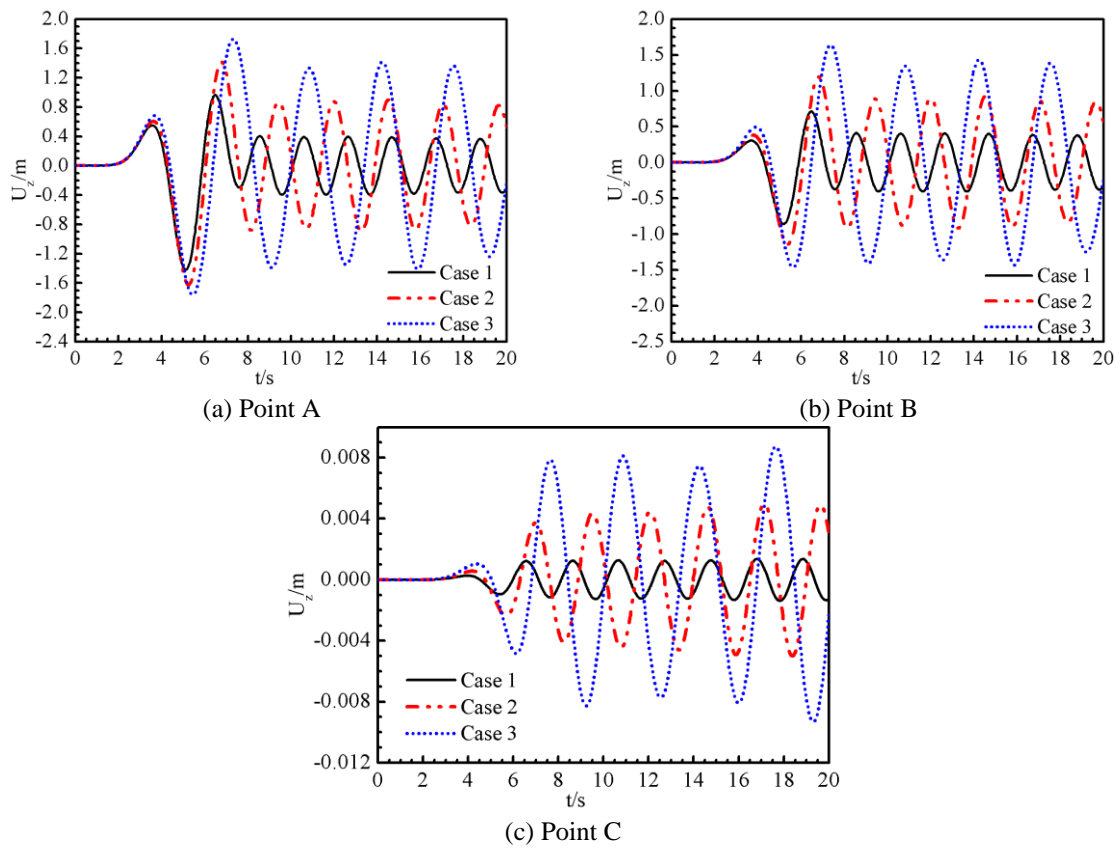

(c) Point C

Fig. 16 Vertical displacements with different shear modulus (in *y*-axis)

three cases, respectively. The mass density and Poisson's ratio of three cases are $\rho_1=\rho_2=1$, $v_1=v_2=0.33$.

As shown in Figs. 16 and 17, the vertical displacement amplitudes increase with the shear modulus ratio increasing. This phenomenon becomes more significant as the depth of point

increases. It can be observed from Figs. 16 and 17 that the effect of shear modulus ratio is obvious. As mentioned above, the biggest amplitudes occur on the surface. It is because that the pulse energy decreases with the depth increasing. In Fig. 16, it depicted the vertical displacement amplitudes of observation point in y-axis. The maximum of the amplitudes for points *A*, *B* and *C* are U_A=1.8, U_B=1.6 and U_C=0.009. It is interesting to note that U_C is obviously smaller than U_A and U_B . The tunnel weakens the wave propagation, so the dynamic response in point *C* is not quite obviously.

As shown in Fig. 17, the shear modulus ratio has a remarkable influence on the vertical displacement of the points in *x*-axis. The vertical displacement amplitudes decrease with the horizontal distance increasing. This is due to the energy decay in the wave propagate process. It is observed that the vertical displacement amplitudes are much bigger than those of the other cases. With the shear modulus ratio increasing, the bottom of the model becomes flexible and this leads to the displacement amplitudes with high shear modulus are much bigger than others. The maximum amplitude of different points did not occur at the same time. It because that there exist the wave reflection and phase angle change.
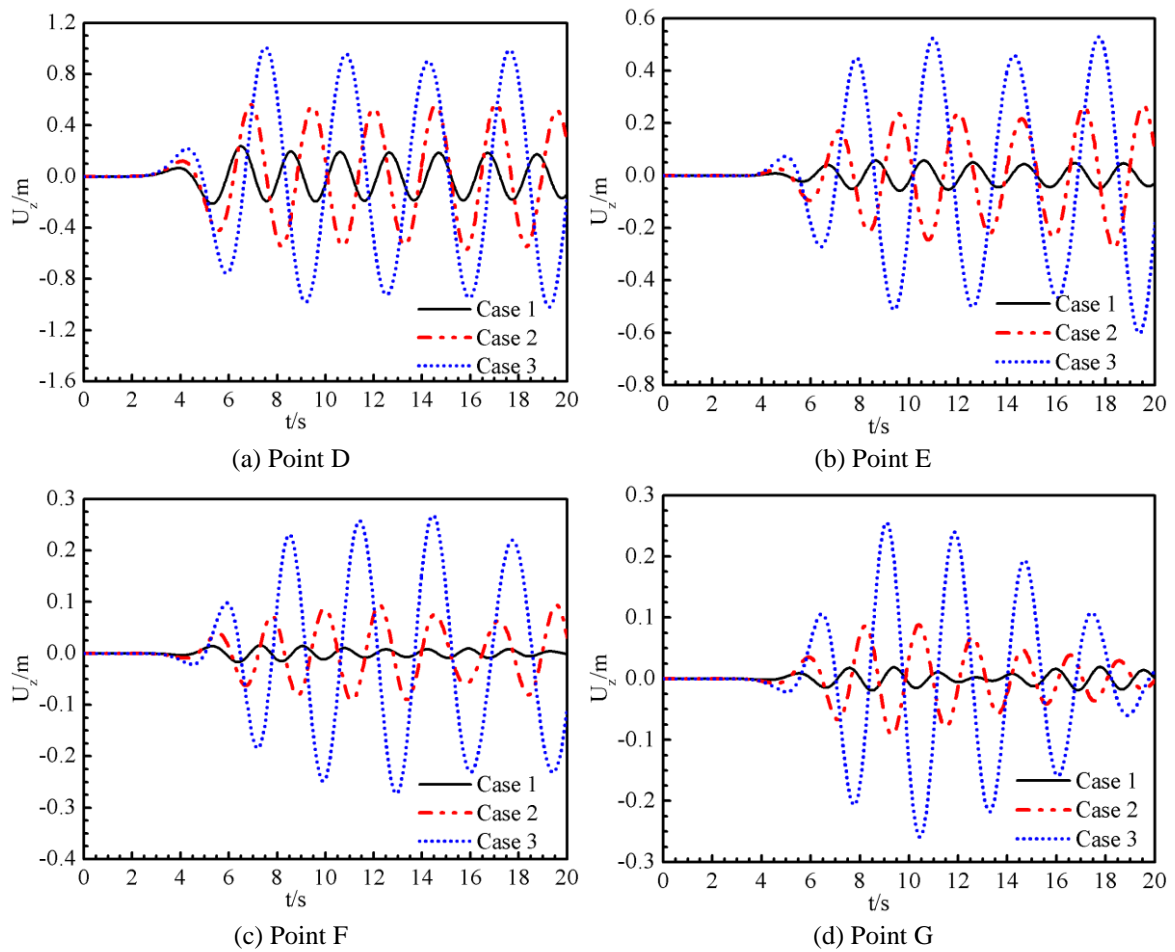

(a) Point D

(b) Point E

(c) Point F

(d) Point G

Fig. 17 Vertical displacements with different shear modulus (in *x*-axis)

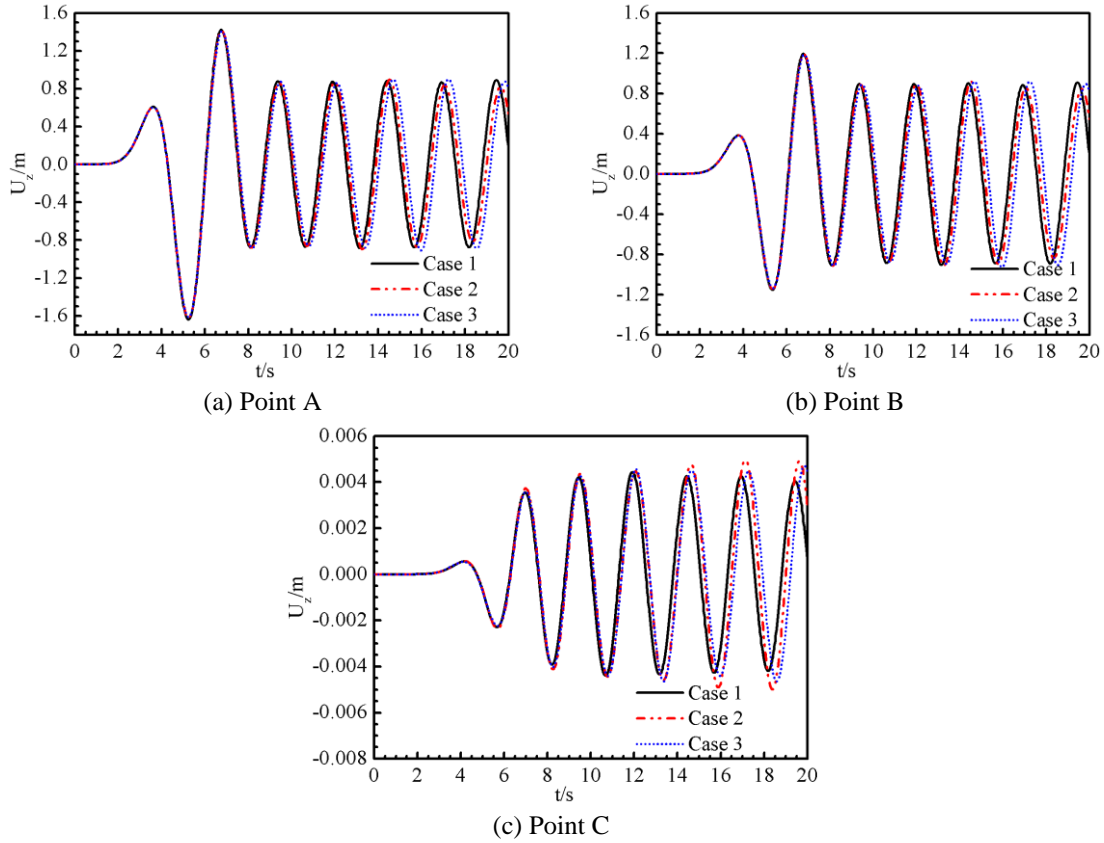(a) Point A

(b) Point B

(c) Point C

Fig.18 Vertical displacements with different mass density (in *y*-axis)

In order to analyze the influence of material parameters on the layered soil model, the mass density ratio $n_\rho = \rho_1/\rho_2$ is selected as a variable quantity. Basing on the control variate method, three cases with various mass density are discussed as follow, case 1: $\rho_1=1$, $\rho_2=0.8$; case 2: $\rho_1=1$, $\rho_2=1$; case 3: $\rho_1=1$, $\rho_2=1.2$. The mass density ratio n_ρ is equal to 1.25, 1.0, 0.83 for three cases, respectively. The other material parameters are the same for the three cases: $G_1=G_2=1$, $v_1=v_2=0.33$. The Ricker wavelet impulse which is exhibited in Fig. 4 acts on observation point A.

As shown in Fig. 18, the differences among three cases are gradually strengthened and more remarkable as the depth of point increases. With the mass density ratio increasing, the vertical displacement amplitudes trend to increase especially for the points in *x*-axis. It can be note that remarkable differences between the points in *y*-axis and *x*-axis exit. The mass density ratio has more obvious influence on the vertical displacement of points in y-axis than the points in *x*-axis. Therefore, the mass density ratio mainly can influence the points in the horizontal direction. For a fixed mass density ratio, the results curves have a phase angle change phenomenon. The reason is that the wave propagates with the distance increasing, and the peak of wave moves.

6.5 Influence of different load forms on dynamic response

In the dynamic analysis of the road system, the vehicle load is often simplified as a
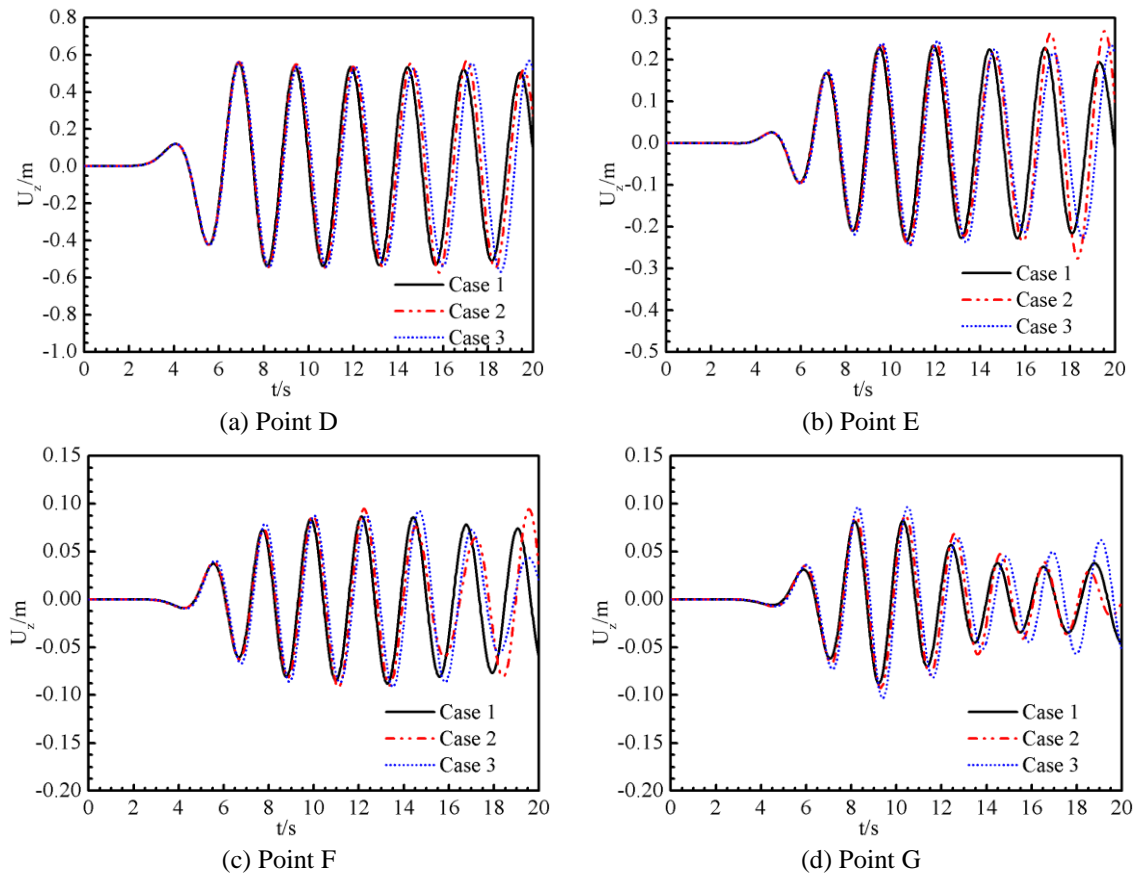
(a) Point D

(b) Point E

(c) Point F

(d) Point G

Fig. 19 Vertical displacements with different mass density (in *x*-axis)

concentrated load or uniform load. Different dynamic characteristics of the soil medium are reflected by different load forms. Therefore, it can be noted that the load forms are worthy attention factor in dynamic analysis. In this section, a single layered medium as shown in Fig. 3 is proposed, and the physical dimension and soil properties are the same as that of section 6.1.1. Only the load form is different. The uniform load and concentrated load are introduced to illuminate the influence of load forms on the dynamic analysis. The concentrated load is the same as the load in section 6.1.1. The uniform load range is from -0.5b to 0.5b (the total thickness of the soil model b=1.), and the amplitude $P(t)$ is defined in Eq. (61). The two kinds of load act on point A in the vertical direction, respectively. The vertical displacements of observation points with different load forms are shown in Fig. 20. For the early times 0.0<t<8.0s, the displacement caused by uniform load is different from that of concentrated load. However, for t>8.0s, the displacements caused by two kinds load form tend to consistent. By comparing Fig. 20(a) and (c), we find that the vertical displacements causing by different load forms converge to each other as the horizontal distance increasing. The phenomenon also can be noted in Fig. 20(b) and (d). According to Saint-Venant's principle, the different load forms only have remarkable influence on dynamic response of the near field. The sphere of influence of two load forms in nearfield is different. Therefore, the load form plays an important role in the nearfield dynamic analysis.
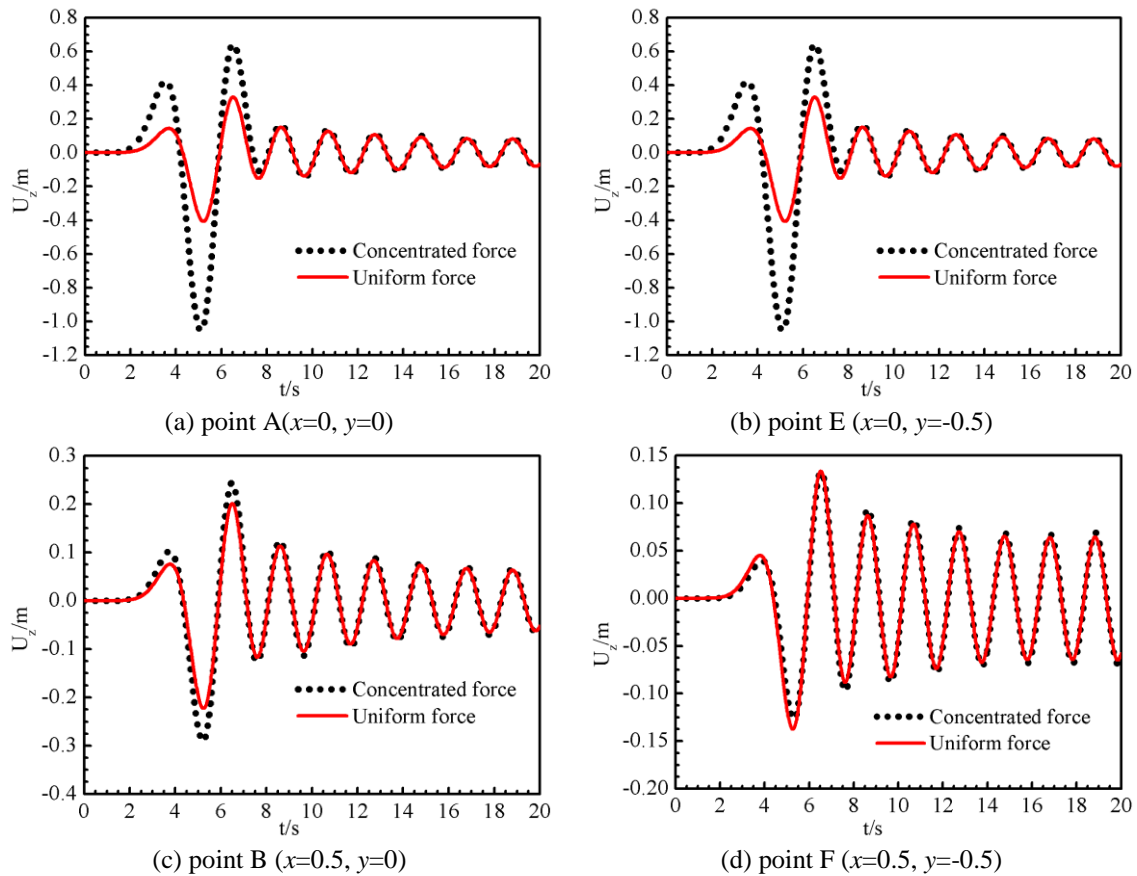
(a) point A(*x*=0, *y*=0)

(b) point E (*x*=0, *y*=-0.5)

(c) point B (*x*=0.5, *y*=0)

(d) point F (*x*=0.5, *y*=-0.5)

Fig. 20 Influence of different load forms on vertical displacement

7. Conclusions

A modified scaled boundary element method in the time domain is derived, which can be used to modeling the unbounded domain with bedrock. It is based on the continued fraction solution of the dynamic stiffness of unbounded domain. Because only the boundary of the unbounded domain is discretized, it leads to a reduction of spatial dimension by one. This leads the computational efficiency to increase. The proposed modified SBFEM in time domain is considered as more suitable to model the multilayered unbounded domain than a reference solution by using the finite element method. The modified SBFEM can be coupled with the finite element method seamlessly by using the same shape function. In this paper, the neafield is modeled by the finite element method and the farfield is modeled by modified SBFEM. The proposed method can be successfully applied to the large-scale systems. The standard motion of equation on structural dynamic is formulated by introducing the familiar static stiffness matrix, mass matrix and the high order expansion terms. In order to make the unstable solution vanish, the spectral shifting technique method is used to deal with the first order equation. According to the coefficient matrices are symmetry and sparse, the standard equation of motion of the linear system can be solved by time-stepping scheme, such as the direct time domain integration method. The

integration method can calculate large number of internal variables at each time step, and the computational efficiency is high.

A single and multi-layered medium are analyzed, respectively. Very good agreements between the viscous-spring solutions and the solutions using the proposed method are obtained. It demonstrates that the proposed method is accurate even in the crude mesh. The influence of material parameters, such as the shear modulus ratio and the mass density ratio, are both considered, respectively. The results reveal that the variable material parameters lead remarkable influence in layered soil model. The shear modulus ratio have more influences on the dynamic response of layered model that the mass density ratio. However, the mass density ratio mainly influences on the horizontal point. Therefore, the material parameters play very important role in the analysis of layered model. The influence of load form on dynamic response for layered medium is also discussed in this paper. On the other hand, due to the tunnel always through layered model, the tunnel plays an important role in the time of rail transit. Different load forms have greatly influence on the dynamic response in near field. Therefore, it is very importance to choose a reasonable simplified load model in dynamic response in future road traffic research. The present study may be easily extended to other promising and unsolved objects, such as three dimensional problem, scalar problem and dam reservoir interaction problem. Those may be the subjects in the future study.

Acknowledgments

References

Adhikari, S. and Wagner, N. (2004), "Direct time-domain integration method for exponentially damped linear systems", *Comput. Struct.*, **82**, 2453-2461.

Ai, Z.Y. and Feng, D.L. (2014), "Analytical layer element solutions for deformations of transversely isotropic multilayered elastic media under nonaxisymmetric loading", *Int. J. Numer. Anal. Meth. Geomech.*, **38**(15), 1585-1599.

Ai, Z.Y. and Cang, N.R. (2012), "Analytical layer-element solutions for a multi-layered transversely isotropic elastic medium subjected to axisymmetric loading", *J. Zhejiang Univ. Sci. A*, **13**(1), 9-17.

Ai, Z.Y. and Li, Z.X. (2014), "Analytical layer-element solution to axisymmetric dynamic response of transversely isotropic multilayered half-space", *Soil Dyn. Earthq. Eng.*, **66**, 69-77.

Ai, Z.Y. and Zhang, Y.F. (2015), "Plane strain dynamic response of a transversely isotropic multilayered half-plane", *Soil Dyn. Earthq. Eng.*, **75**, 211-219.

Ai, Z.Y. and Cheng, Y.C. (2011), "Analytical layer-element solution to axisymmetric consolidation of multilayered soils", *Comput. Geotech.*, **38**(2), 227-232.

Bazyar, M.H. and Song, C. (2008), "A continued-fraction-based high-order transmitting boundary for wave propagation in unbounded domains of arbitrary geometry", *Int. J. Numer. Meth. Eng.*, **74**(2), 209-237.

Beskos, D.E. (1987), "Boundary element methods in dynamic analysis", *Appl. Mech. Rev.*, **40**(1), 1-23.

Birk, C. and Song, C. (2009), "A continued-fraction approach for transient diffusion in unbounded medium", *Comput. Meth. Appl. Mech. Eng.*, **198**, 2576-2590.

Birk, C., Prempramote, S. and Song, C. (2010), "High-order doubly asymptotic absorbing boundaries for the acoustic wave equation", *Proceedings of 20th International Congress on Acoustics*, Sydney, Australia.

Birk, C. and Song, C. (2010), "A local high-order doubly asymptotic open boundary for diffusion in a semiinfinite layer", *J. Comput. Physica*, **229**, 6156-6179.

Birk, C., Prempramorte, S. and Song, C. (2012), "An improved continued-fraction-based high-order transmitting boundary for time-domain analyses in unbounded domains", *Int. J. Meth. Eng.*, **89**(3), 269-298.

Birk, C. and Behnke, R. (2012), "A modified scaled boundary finite element method for three-dimensional dynamic soil-structure interaction in layered soil", *Int. J. Meth. Eng.*, **89**, 371-402.

Bycroft, G.N. (1956), "Forced vibrations of a rigid circular plate on a semi-infinte elastic space and on an elastic stratum", *Phil Tran. R. Soc.*, *London, Ser. A*, **248**, 327-368.

Chen, D. and Birk, C. (2014), "A high-order approach for modeling transient wave propagation problems using the scaled boundary finite element method", *Int. J. Numer. Meth. Eng.*, **97**(13), 937-959.

Chen, D. and Du, C.B. (2014), "A computational model for structure-foundation dynamic interaction in time domain", *Chin. J. Rock Soil Med.*, **4**(35), 1164-1172.

Chen, D. and Dai, S.Q. (2014), "A high-order time-domain model of dam-foundation dynamic interaction", *Chin. J. Hyd. Eng. ShuiLi Xuebao*, **45**(5), 60-70.

Deeks, A.J. and Randolph, M.F. (1994), "Axisymmetric time-domain transmitting boundaries", *J. Eng. Mech.*, ASCE, **120**(1), 25-42.

Fan, S.C., Li, S.M. and Yu, G.Y. (2005), "Dynamic fluid-structure interaction analysis using boundary finite element method-finite element method", *J. Appl. Mech.*, ASME, **72**, 591-598.

Genes, M. (2012), "Dynamic analysis of large-scale SSI systems for layered unbounded media via a parallelized coupled finite element/boundary-element/scaled boundary finite-element model", *Eng. Anal. Bound. Elem.*, **36**, 845-857.

Hall, W.S. and Oliveto, G. (2003), *Boundary Element Methods for Soil-Structure Interaction*, Kluwer Academic Publishers, Dordrecht.

Kausel, E. and Roesset, J.M. (1975), "Dynamic stiffness of circular foundations", *J. Eng. Mech. Div.*, **101**, 771-785.

Kausel, E. and Peek, R. (1982), "Dynamic loads in the interior of a layered stratum: an explicit solution", *Bul. Seismol. Soc. Am.*, **72**, 1459-1481.

Kausel, E. (1986) "Wave propagation in anisotropic layered media", *Int. J. Numer. Meth. Eng.*, **23**, 1567-1578.

Kausel, E. (1994), "Thin-layer method: formulation in the time domain", *Int. J. Numer. Meth. Eng.*, **37**, 927-941.

Komatitsch, D. and Tromp, J. (2002), "Spectral-element simulations of global seismic wave propagation-I. Validation", *Geophy. J. Int.*, **149**(2), 390-412.

Laub, A.J. (1979), "A Schur method for solving algebraic Riccati equations", *IEEE Tran. Auto. Control*, **AC-24**, 913-921.

Lehmann, L. and Ruberg, T. (2006), "Application of hierarchical matrices to the simulation of wave propagation in fluids", *Commun. Numer. Meth. Eng.*, **22**, 489-503.

Lin, G., Liu, J., Li, J.B. and Fang, H.Y. (2011), "Scaled boundary finite element approach for waveguide eigenvalue problem", *IET Microw. Anten. Propag.*, **12**(5), 1508-1515.

Liu, J.B., Gu, Y. and Du, Y.X. (2006), "Consistent viscous-spring artificial boundaries and viscous-spring boundary elements", *Chin. J. Geotech. Eng.*, **28**(9), 1070-1075.

Liu, J.B., Du, Y.X. and Du, X.L. (2006), "3D viscous-spring artificial boundary in time domain", *Earthq. Eng. Eng. Vib.*, **5**, 93-102.

Murakami, A., Fukui, M. and Hasegawa, T. (1996), "Deformation analysis and bearing capacity of two-layered soil deposit with a surface crust considering couple stresses", *Soil. Found.*, **36**(3), 133-139.

Richart, F.E. and Whitman, R.V. (1967), "Comparison of footing vibration tests with theory", *J SM*, ASCE, **93**(6), 65-91.

Radmanovic, B. and Kata, C. (2010), "A high performance scaled boundary finite element method", *IOP Conference Series: Material Science and Engineering*, **10**, 1-10.

Schauer, M. (2012), "Parallel computation of 3-D soil-structure interaction in time domain with a coupled FEM/SBFEM approach", *J. Sci. Comput.*, **52**, 446-467.

Seale, S.H. and Kausel, E. (1989), "Point loads in cross-anisotropic layered halfspaces", *J. Eng. Mech.*, **115**, 509-542.

Song, C. and Wolf, J.P. (1995), "Consistent infinitesimal finite-element-cell method: out-plane motion", *J. Eng. Mech.*, **121**, 613-619.

Song, C. and Wolf, J.P. (1996), "Consistent infinitesimal finite-element-cell method: three-dimensional vector wave equation", *Int. J. Numer. Meth. Eng.*, **39**, 2189-2208.

Song, C. and Wolf, J.P. (1997), "The scaled boundary finite-element method-alias consistent infinitesimal finite-element cell method-for elastodynamics", *Comput. Meth. Appl. Mech. Eng.*, **147**, 329-355.

Song, C. and Wolf, J.P. (2000), "The scaled boundary finite-element-a primer: solution procedures", *Comput. Struct.*, **78**, 211-225.

Song, C. (2004), "A matrix function solution for the scaled boundary finite-element equation in statics", *Comput. Meth. Appl. Mech. Eng.*, **193**, 2325-2356.

Song, C. and Bazyar, M.H. (2007), "A boundary condition in the Padé series for frequency domains solution of wave propagation in unbounded domains", *Int. J. Numer. Meth. Eng.*, **69**, 2330-2358.

Song, C. (2011), "The scaled boundary finite element method in structural dynamics", *Int. J. Numer. Meth. Eng.*, **31**, 1724-1732.

Sung, T.Y. (1953), "Vibration in semi-infinite solides dur to periodic surface loading", *ASTM-STP, No. 156, Symposium on Dynamic Testing of Soil*, 35-64.

Trinks, C. (2004), "Consistent absorbing boundaries for time-domain interaction analyses using the fractional calculus", PhD Thesis, Technische Universität Dresden, Fakultät Bauingenieurwesen.

Wolf, J.P. and Song, C. (1995), "Consistent infinitesimal finite-element-cell method: in-plane motion", *Comput. Meth. Appl. Mech. Eng.*, **123**, 355-370.

Wolf, J.P. and Song, C. (1997), "Finite-element modelling of unbounded media", *Earthq. Eng. Struct. Dyn.*, **26**(6), 667-668.

Wolf, J.P. (2003), *The Scaled Boundary Finite Element Method*, Wiley & Sons, Chichester.

Yan, J., Zhang, C. and Jin, F. (2004), "A coupling procedure of FE and SBFE for soil- structure interaction in the time domain", *Int. J. Numer. Meth. Eng.*, **59**, 1453-1471.

Zhang, X., Wegner, J.L. and Haddow, J.B. (1999), "Three-dimensional dynamic soil-structure interaction analysis in the time-domain", *Earthq. Eng. Struct. Dyn.*, **28**, 1501-1524.

Zhao, C.B. (2009), *Dynamic and transient infinite elements; Theory and geophysical, geotechnical and geonvironmental applications*, Springer, Berlin.

CC